The growth of amyloid fibrils: rates and mechanisms

Büll, Alexander K.

Published in:
Biochemical Journal

Link to article, DOI:
10.1042/BCJ20160868

Publication date:
2019

Document Version
Publisher's PDF, also known as Version of record

Biochemical Journal (2019) **476** 2677–2703
https://doi.org/10.1042/BCJ20160868

PORTLAND PRESS

Review Article

The growth of amyloid fibrils: rates and mechanisms

Alexander K. Buell*

Department of Biotechnology and Biomedicine, Technical University of Denmark, 2800 Kgs. Lyngby, Denmark

Correspondence: Alexander K. Buell (alebu@dtu.dk)

Amyloid fibrils are β-sheet-rich linear protein polymers that can be formed by a large variety of different proteins. These assemblies have received much interest in recent decades, due to their role in a range of human disorders. However, amyloid fibrils are also found in a functional context, whereby their structural, mechanical and thermodynamic properties are exploited by biological systems. Amyloid fibrils form through a nucleated polymerisation mechanism with secondary processes acting in many cases to amplify the number of fibrils. The filamentous nature of amyloid fibrils implies that the fibril growth rate is, by several orders of magnitude, the fastest step of the overall aggregation reaction. This article focusses specifically on *in vitro* experimental studies of the process of amyloid fibril growth, or elongation, and summarises the state of knowledge of its kinetics and mechanisms. This work attempts to provide the most comprehensive summary, to date, of the available experimental data on amyloid fibril elongation rate constants and the temperature and concentration dependence of amyloid fibril elongation rates. These data are compared with those from other types of protein polymers. This comparison with data from other polymerising proteins is interesting and relevant because many of the basic ideas and concepts discussed here were first introduced for non-amyloid protein polymers, most notably by the Japanese school of Oosawa and co-workers for cytoskeletal filaments.

Introduction

The formation of amyloid fibrils is a multi-step process, involving nucleation, growth and proliferation steps [1] (Figure 1a). It is of an obvious interest to understand how and why the first fibril(s) nucleate in a given system [2] and how they proliferate through secondary processes [1,3]. However, the nature of amyloid fibrils, as protein polymers of very high aspect ratio (ratio length/width) of up to 1000 and more, underlines the dominant role that fibril growth plays in the overall conversion process of monomeric to fibrillar protein. Amyloid fibril growth, the addition of a (monomeric) building block onto a fibril end, corresponds to a basic manifestation of the phenomenon of misfolding [4]: the protein monomer inside the fibril adopts a non-native conformation into which it has to 'mis'-fold (Figure 1a, b). Much general insight into protein aggregation can be gained from the selective and careful study of amyloid fibril growth in isolation. It is, therefore, somewhat surprising that the number of published studies that have put some emphasis on the detailed studies of fibril growth represent only a small fraction of the overall literature on amyloid fibrils. The aim of this article is to summarise the general state of knowledge on the kinetics and mechanisms of amyloid fibril growth. The perspective will be hereby limited entirely to experimental studies, reflecting the author's own limitations in being able to assess computational work. Furthermore, the small number of available analytical theoretical treatments of fibril elongation have been excluded from the discussion, which does in no way express any negative attitude towards these types of studies. On the contrary, I hope that the extensive collection of data that I have gathered for this article will trigger the interest of theoreticians and provide them with a basis for the further conceptual development of amyloid fibril elongation. Furthermore,

*Alexander K. Buell was the recipient of the Biochemical Society's Biotechnology Early Career Research Award in 2017.

Received: 2 August 2019
Revised: 8 September 2019
Accepted: 10 September 2019

Version of Record published: 11 October 2019

Biochemical Journal (2019) 476 2677–2703
https://doi.org/10.1042/BCJ20160868

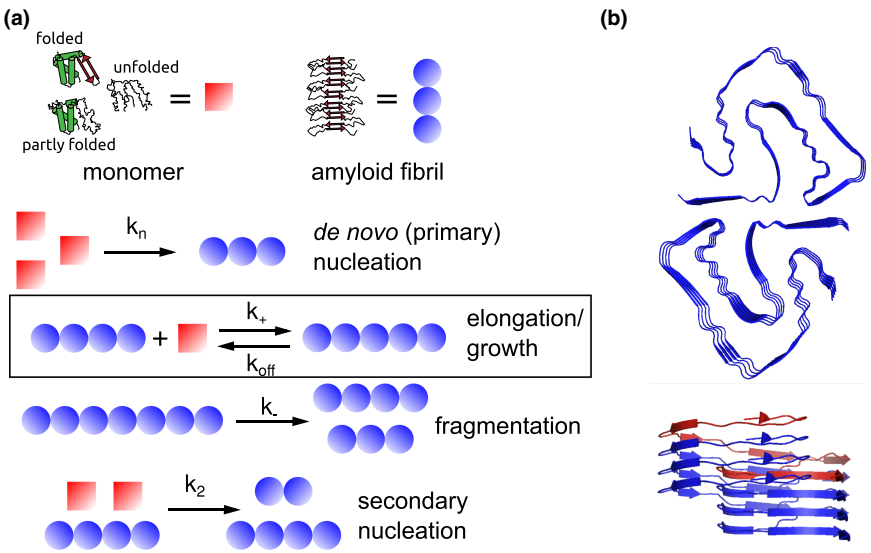

Figure 1. Amyloid fibril growth—a key step in the aggregation pathway.

(**a**) The transition from monomeric protein towards an amyloid fibril is a multi-step process, consisting of nucleation, growth and proliferation steps. This article focusses specifically on the growth, or elongation, of the fibrils. (**b**) Emerging atomic resolution structural information on amyloid fibrils (illustrated with amyloid fibrils from PI3K-SH3 [9] pdb 6R4R) demonstrates that the picture of amyloid fibrils as purely one-dimensional assemblies is an oversimplification. Top: cross-section of the fibril, which consists of two identical filaments. Bottom: side view of a small filament segment, illustrating that each monomeric building block (see monomer marked in red) spans several layers of the filament.

I hope that this article will stimulate additional experimental research on amyloid fibril elongation that will help in elucidating both the governing general physico-chemical principles at work and the specific features that each unique fibril system presents. In particular, the latter is being finally enabled through the increased availability of high-resolution structures of amyloid fibrils, mostly from cryo-electron microscopy (cryo-EM, Figure 1b) [5–9]. In the following treatment, the implicit assumption is made that above a certain length, the elongation (and dissociation) rate constant of an amyloid fibril is independent of the length of the fibril. While this is a plausible assumption, given the high degree of order and periodicity of amyloid fibrils, it is very challenging to determine the length of such a minimal fibril experimentally. However, the emerging high-resolution structural information allows at least to define a minimal unit within which the monomer at an extremity can undergo the same interactions as in an infinitely long fibril [7,9]. Therefore, when I speak of amyloid fibrils in the following, I always mean a structure of at least the size of this minimal unit.

Experimental measurements of amyloid fibril growth

The study of amyloid fibril growth relies on the availability of an experimental probe that is able to distinguish between protein molecules in their monomeric/soluble form and their fibrillar form. The most widely used methods investigate amyloid fibril formation and growth in solution and are spectroscopic in nature, notably based on fluorescent dye molecules that have distinct affinities and fluorescence spectral properties when exposed to either monomeric or fibrillar protein. Next to the most commonly used dye Thioflavin-T, several others have been developed [10], but none of these has as yet been able to replace ThT as the dye of choice of most research groups in this field. Its use has been extensively reviewed elsewhere [11]. The fact that amyloid fibril growth is usually associated with a notable increase in β-sheet content allows also the use of circular dichroism (CD) spectroscopy [12]. The formation of aggregates is, in general, associated with a strong increase in light scattering, due to the R^6 scaling of the Rayleigh scattering intensity with the particle radius R, in the case of a spherical particle. While this increase in scattering can be problematic in spectroscopic experiments, it can be directly exploited in light scattering experiments to follow amyloid fibril formation in general [13] and fibril growth rates in particular [14], because the overall scattering intensity is dominated by the aggregates, even under conditions where monomer is present at a large excess. Furthermore, the kinetics of amyloid fibril

growth can be followed through the heat that is released or absorbed during the growth reaction, using isothermal titration calorimetry (ITC) [15]. However, these types of experiments have mainly been used so far for thermodynamic [16,17] rather than kinetic studies.

Another important class of measurement techniques for protein aggregation, which are particularly well adapted for studying the growth of pre-formed fibrils, are surface-based biosensing experiments, whereby the seed fibrils are attached to the surface of a biosensor [18], allowing only processes in proximity to the surface to be detected. The growth of the surface-bound fibrils upon exposure to protein solutions can then be monitored. Under optimised conditions, the sensor surface needs to be incubated with solutions of protein monomer only for several minutes, a time scale during which, in most cases, no significant nucleation of new fibrils occurs. The use of surface-based biosensing for the study of amyloid fibril growth was initially mostly based on surface plasmon resonance (SPR [19–21], detection based on change in refractive index), but later, quartz crystal microbalance (QCM [22,23], detection based on change in hydrodynamic mass) devices were shown to allow the convenient and detailed study of amyloid fibril growth. It has been shown that, at least concerning the relative effects of changes in salt concentration on the fibril elongation rate, surface-based biosensing techniques (SPR and QCM) are equivalent to bulk solution techniques [dynamic light scattering (DLS), ThT fluorescence] [14].

Independently of the physical principle used to follow the growth of amyloid fibrils, two fundamentally different types of measurements of amyloid fibril growth rates can be distinguished, those based on monitoring a large number of simultaneously growing fibrils (ensemble measurements), and those where the growth of individual fibrils is studied (single particle measurements). While the majority of available data on amyloid fibril growth have been obtained using ensemble experiments, single particle experiments can provide unique and detailed mechanistic insight. In the section on the energy barriers of amyloid fibril growth, I discuss in more detail the different types of information provided by ensemble and single particle experiments and how they can be compared.

When an individual amyloid fibril is monitored over time, for example by atomic force microscopy [24–29] or high-resolution optical microscopy [30–32], the growth rate can be directly extracted from the so-called kymographs, i.e. plots of fibril length against time. The most recent additions to the array of single particle techniques applicable to the study of amyloid fibrils are interferometric scattering microscopy (iSCAT) [33], whereby the scattering intensities from individual particles are measured, and thermophoretic traps, where individual amyloid fibrils can be trapped and observed by fluorescence microscopy [34]. In ensemble measurements, the average behaviour of a large number of fibrils is studied and a detailed kinetic analysis of the data is necessary in order to be able to extract fibril growth rates. When *de novo* aggregation experiments are carried out, starting with fully monomeric protein, global fitting of concentration-dependent kinetic data is necessary in order to determine the rates and rate constants of the individual nucleation, growth and proliferation processes [35]. This situation can be dramatically simplified by performing strongly seeded experiments, in which fibril elongation is the only process that contributes significantly to the reaction [36]. The regime of strong seeding can be achieved in one of two ways. In solution experiments, a sufficient quantity of seeds has to be added, such that during the timescale of consumption of the monomeric protein, no significant increase in the number of fibrils occurs due to *de novo* nucleation. This may mean adding between 1 and 50% of seed fibrils (mass equivalents) to the monomeric protein at the start of the reaction [36,37]. The strongest criterion for assessing whether or not processes in addition to fibril elongation occur in a given seeded reaction is to fit the resulting data to a kinetic model. If the full aggregation time course corresponds to a single exponential function (see Appendix 1 for a derivation), it is very likely that only elongation contributes appreciably to the dynamic behaviour of the aggregating system.

All seeded experiments have in common that the seed preparation is of crucial importance for the quality and reproducibility of the data. Homogenisation by stirring or treatment with ultrasound [38] is of great benefit and it is recommended to characterise the seed fibrils by a high-resolution imaging technique, such as AFM or EM (negative staining or cryogenic). Even though the purity of the monomeric protein is always an important point in biophysical studies of amyloid fibrils, contamination with small amounts of aggregates that can act as seeds is of less consequence in strongly seeded compared with unseeded experiments, because the strong seeding will dominate the behaviour and mask the influence of any potential weak contamination in the monomer. In a section further below, I propose a definition of a way to quantify the seeding efficiency of a given batch of fibrils, which can contribute to rendering data acquired with different batches of seed fibrils more easily comparable.

The concentration-dependence of amyloid fibril growth

In the study of any reaction mechanism, the most basic and yet one of the most insightful experiments is a variation of the concentration of the reactants. As outlined above, the reagents of an amyloid fibril growth

Biochemical Journal (2019) **476** 2677–2703
https://doi.org/10.1042/BCJ20160868

experiment are monomeric protein and pre-formed seed fibrils. Both can be varied, but the variation of the concentration of seed fibrils is more limited in range. When the concentration of added seed fibrils is very low, the time scale of the seeded experiment can become too long to allow the neglecting of nucleation processes during the course of the experiment. At very high seed concentrations, on the other hand, the reaction can be too fast to reliably measure with conventional equipment, such as fluorescence multiwell plate-readers, and higher order assembly of fibrils can rapidly become relevant [37]. Therefore, in practice, seed fibril concentrations in bulk solution experiments rarely exceed small micromolar concentrations. In such experiments, the expected linear dependence of the overall growth rate with seed concentration is usually found [37,39–43]. Monomer concentration, on the other hand, can be varied by several orders of magnitude, ranging from sub-micromolar to hundreds of micromolar.

Two fundamental observations have been made about the concentration-dependence of amyloid fibril growth. At very low concentrations (often below micromolar), fibrils can be observed to cease to grow, and even dissociate in some cases (negative elongation rate in Figure 2). This behaviour is easily explained through the fact that amyloid fibrils are in equilibrium with monomeric protein and if the available monomer concentration falls below the equilibrium concentration (m_{eq}), also known as critical concentration (m_{crit}) the equilibrium shifts in the direction of the monomer, which corresponds to dissociation of fibrils (Figure 2a). This characteristic behaviour has been used repeatedly to determine the equilibrium concentration of functional protein polymers, such as actin [44,45] and tubulin [46]. In the case of amyloid fibrils, such studies at very low monomer concentrations are most easily performed using surface-based experimental techniques. In a bulk solution experiment, very low monomer concentrations can only be achieved by strongly diluting an equilibrated, fibrillar sample, which renders subsequent characterisation difficult. In a surface-based experiment, the solution in equilibrium with the surface-bound fibrils can be easily and rapidly replaced by a more dilute solution, or indeed pure buffer using the flow system of the biosensing device. By decreasing the monomer concentration in contact with the seeds to very low values and measuring in each case the rate of growth or dissociation, the equilibrium concentration of monomer can be determined [20,29,47]. In these types of experiments at low monomer concentrations, linear behaviour of the growth rate, as a function of the monomer concentration, is usually found, in agreement with the idea that fibril growth is a bimolecular reaction between a monomer and a fibril end [37,39,48,49]. Indeed, if amyloid fibrils were to grow by the addition of dimers or larger oligomers in equilibrium with monomers, a higher than linear dependence of the growth rate on the concentration of soluble protein can be expected, as has recently been reported for the first time in the case of the ΔN6 variant of β2-microglobulin [50]. Therefore, a careful examination of the concentration dependence of amyloid fibril growth rates at low concentration allows us to define the elongating species. It should be noted, however, that while amyloid fibrils have been found to grow in most cases by monomer addition, monomer refers in this context to the smallest existing unit in solution, which could, in fact itself be a dimer or higher order structure, such as is the case for insulin for example, where under many conditions the only species that is detectable is the dimer [51] and only relatively harsh conditions lead to monomerisation [51].

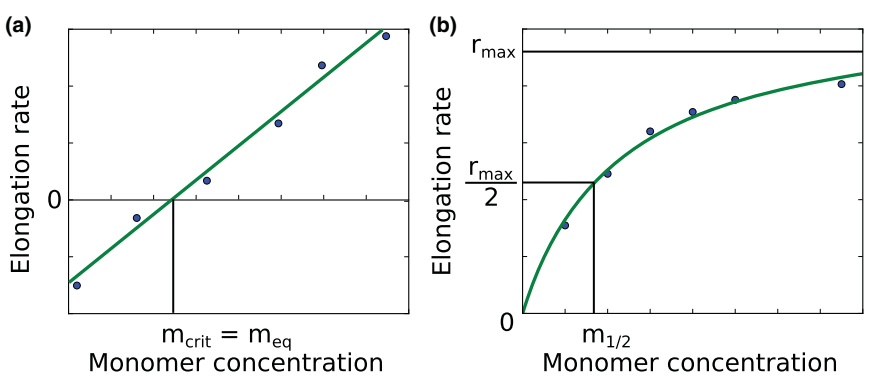

Figure 2. Illustrations of the dependence of the amyloid fibril elongation rate on monomer concentration. (**a**) Low concentration regime, whereby the equilibrium or critical concentration can be determined as the concentration at which no net growth is observed. (**b**) High concentration regime, where it is found that the fibril growth rate eventually reaches saturation, i.e. further increase in the concentration does not lead to a further increase in elongation rate.

Biochemical Journal (2019) 476 2677–2703
https://doi.org/10.1042/BCJ20160868

The critical concentration for fibril growth can depend strongly on the solution conditions [53], but is generally quite low (often significantly below one micromolar, for example in the case of the amyloid β-peptide [20,53,54]), which explains that not many accurate measurements are available. One amyloid protein for which a wide variety of reports for the critical concentration exist is α-synuclein. It is often reported that at the end of aggregation experiments, up to several tens of micromolar of non-fibrillar protein is detected [43,55], for example by measuring the concentration of the supernatant solution after centrifugation. At the same time, it has been reported that α-synuclein can aggregate in solution at low micromolar concentrations [56] and from lipid bilayers at low nanomolar concentrations [57]. Therefore, reports for the critical concentration span more than three orders of magnitude in this system, corresponding to apparent differences in aggregate stability of more than 17 kJ/mol. This difference can be explained by the fact that in some experiments, thermodynamic equilibrium may not have been reached yet [55], whereby the measured monomer concentration does not correspond to the equilibrium concentration. On the other hand, the finding that fibrillar aggregates can form at very low monomer concentrations from lipid bilayers could stem from an additional stabilisation that the fibrils gain by forming protein-lipid co-aggregates. Furthermore, the effective concentration close to a surface which has a high affinity for the protein can also be substantially higher than the bulk concentration.

On the other end of the spectrum is the exploration of the amyloid fibril elongation behaviour at high monomer concentrations. Most studies that have explored a sufficiently large concentration range have found that the linear dependence of the growth rate observed at low monomer concentrations eventually goes over into a regime whereby the elongation rate becomes independent of monomer concentration (Figure 2b). This transition from linear to saturated behaviour is reminiscent of Michaelis–Menten enzyme kinetics, as had already previously been pointed out in the case of the concentration dependence of flagellin polymerisation [58]. The fibril ends correspond to the enzymes' active sites and the monomer concentration corresponds to the substrate concentration. Similarly to the case of enzyme kinetics, this type of concentration dependence can be characterised by the concentration at which half the maximal elongation rate is reached, $m_{1/2}$. This characteristic concentration has been measured for a range of amyloid systems (see Table A1 in Appendix 2 for numerical values and references), but no comparative analysis of the available data has been performed to date. In Figure 3a, these concentrations are compared for a range of systems by plotting $m_{1/2}$ against the length of the polypeptide chain. Using dimensionality arguments, $m_{1/2}$, can be converted into a time scale (Figure 3b, see Appendix 2 for details), which we have shown previously to correspond to a residency time, τ_r of the protein monomer at the fibril end [48].

It appears as if $m_{1/2}$, respectively τ_r, are weakly correlated with sequence length, with longer sequences spending on average more time in proximity of the fibril end. While the fibril end is occupied by a monomer, no other protein molecule can attempt an incorporation, and therefore a longer residency time corresponds to a lower saturation concentration. However, it is also apparent that a given protein can display a wide variation of different τ_r under different solution conditions (Table A1). This phenomenon is most clearly illustrated by the results of a recent study, whereby amyloid fibril elongation of the mammalian prion protein (PrP) was investigated at a wide variety of different denaturant concentrations and it was found that the saturation behaviour depends dramatically on the denaturant concentration [42]. In Figure 3, only data from one intermediate denaturant concentration (2.3 M GndHCl) are shown. While not enough data of this type exist yet to draw a definitive conclusion, it appears as if in those systems where a dependence of $m_{1/2}$, respectively τ_r on the solution conditions has been investigated, solution conditions that disfavour weak interactions (low pH, no salt [59] or high denaturant concentration [42]) lead to shorter residency times of the monomer at the fibril end. This suggests that the residency time of the monomer at the fibril end is determined by weak and transient interactions with the fibril end. The weak correlation between sequence length and residency time might then stem from the fact that larger sequences can, on average, form a larger number of weak interactions with the fibril end.

Transient vs. steady-state measurements of amyloid fibril growth

The large majority of bulk solution amyloid fibril elongation experiments are performed in a regime of steady-state growth, i.e. during a situation, whereby the concentration of growing fibril ends is much lower (by two to three orders of magnitude) than that of available monomers, and the latter changes only slowly (minutes to hours) during the experiment. This also means that the signal to be detected stems from all the species present in the reaction mixture. When a probe sensitive for the fibrillar state is used, such as ThT, the

Biochemical Journal (2019) 476 2677–2703
https://doi.org/10.1042/BCJ20160868

signal will be dominated by the fibrils, and if the experiment is sensitive to the monomer (e.g. solution nuclear magnetic resonance, NMR), the signal will be dominated by the non-incorporated free monomer. It is very challenging to perform measurements sensitive to the monomer during the process of incorporation into a fibril. Early SPR-based studies have observed that surface-bound fibrils display two kinetic phases upon both exposition to monomeric protein, as well as subsequent washing with a buffer [19–21,60] and this behaviour was interpreted in the framework of the so-called dock–lock model of amyloid fibril growth. In this picture, the monomer attaches initially weakly and reversibly to the fibril end ('dock'), followed by a structural rearrangement and adoption of the fibrillar conformation ('lock'). While this model is in agreement with the data presented in the previous section (saturation of elongation rate at high monomer concentrations), the biphasic behaviour observed in these SPR experiment (illustrated in Figure 4b) cannot be explained in this manner. The amyloid fibrils attached to the SPR sensor surface all contain of the order of hundreds of monomers and therefore 'docking' of a single monomer to each end should lead to a reversible amplitude of less than one per cent of the total surface-bound mass. In these experiments, however, it is usually found that the reversible amplitude represents a much larger (by one order of magnitude and more) fraction of the total surface-bound mass. This finding can be easily explained by assuming that the monomer weakly absorbs not selectively to the fibril ends, but rather to the entire fibril surface (Figure 4). Indeed, a similar conclusion was reached in an elegantly designed study, in which the transient binding of monomeric β2-microglobulin to (non-fluorescent) seed fibrils was followed by Trp fluorescence [61]. It was found that the stoichiometry of monomer binding to fibrils was such that binding to fibril surfaces had to be the dominant process.

In recent years, it has become increasingly evident that the binding of monomeric protein to the surface of fibrils plays a crucial role in the amplification of fibrils through secondary nucleation. Indeed, the thermodynamics of monomer binding to the fibril surface defines the thermodynamics of the overall secondary nucleation behaviour [62,63]. Re-evaluation of previously published data [19–21] within this framework shows that the reported behaviour (scaling of reversible amplitude with incubation time and monomer concentration) is consistent with the picture that upon contact between fibrils and monomer solutions, a rapid pseudo-equilibrium is established between free monomer and monomer weakly associated with binding sites on the fibril surface, which is also consistent with recent QCM experiments [64,65]. The shorter the incubation period with monomer solution, the greater the bias towards (weak, readily reversible) surface attachment and the longer the incubation time, the greater the bias towards (less reversible) elongation (Figure 4). This behaviour has been investigated in some detail for the amyloid β peptide and it has been found that the affinity of the monomer for the fibril surface is ~100 times weaker than for the fibril end [62,63].

Therefore, in order to explore the transient behaviour of monomers in contact with fibril ends and follow the process of incorporation into the fibril, it will be necessary to tune the solution conditions such that monomer has a negligible affinity for the fibril surface, which will be challenging, or else the signal will likely be dominated by binding to the fibril surface, due to the larger number of possible binding sites. Alternatively, single particle/molecule experiments could be designed, whereby the end of a fibril should be selectively monitored over time while exposed to, for example fluorescently labelled monomer. The conformational change of the monomer undergoing incorporation could be followed by, for example, Förster resonance energy transfer (FRET).

The rate constants of amyloid fibril elongation

In Figure 3, it can be seen that the time scales corresponding to the saturation of the elongation process, i.e. the residency times, differ by approximately two orders of magnitude between all the amyloid systems characterised so far. This represents a significantly smaller relative variation compared with that found for the absolute rates of amyloid fibril growth by different proteins, as expressed by the second-order rate constant k_+. This is illustrated in Figure 5, where, without any claim or ambition for completeness, I have gathered data from many studies that either directly quoted a value of k_+ or that allowed to estimate it in a straightforward manner from the presented data, assuming in all cases that growth occurred through monomer addition. Data from both ensemble and single particle experiments are included; the latter allow a direct determination of the fibril growth rate, simply as a measured increase in length over a certain time period.

In ensemble measurements, the detected signal stems from the simultaneous growth of a large number of amyloid fibrils. The data in the plot have been separated into disease-related and functional amyloid. For comparison, rate constants of some non-amyloid functional protein polymers (actin, tubulin and flagellin) are also included, as well as the growth rates of sickle haemoglobin polymers as a representative of non-amyloid disease-related protein polymers.

Biochemical Journal (2019) **476** 2677–2703
https://doi.org/10.1042/BCJ20160868

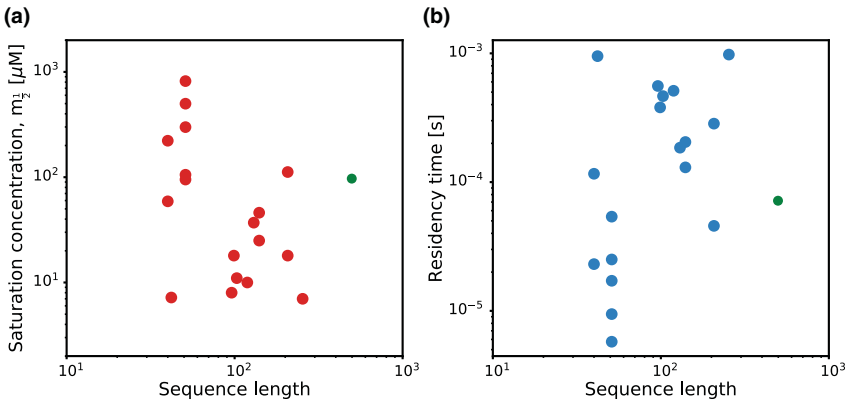

Figure 3. Overview over the saturation concentrations for amyloid fibril elongation reported in the literature. (**a**) The concentration $m_{1/2}$, i.e. the concentration at which the elongation rate reaches half its limiting value, is plotted against the sequence length of the corresponding protein in a double logarithmic plot. (**b**) The values of $m_{1/2}$ have been converted into a characteristic time scale, a residency time τ_r [48] (see Appendix 2 for details). The green data point corresponds in both cases to the value determined for the growth of flagellin filaments [58], a functional polymerising protein system. The data plotted in this figure are summarised in Table A1.

The bi-molecular nature of amyloid fibril elongation, as a reaction between a protein monomer and a fibril end, requires both the concentrations of monomers and fibril ends to be known in addition to the actual reaction rate, in order to be able to determine the magnitude of the molecular rate constant. In this context, the largest uncertainty stems from the determination of the number of growing fibril ends, which is usually based on the analysis of the length distribution of the seed fibrils by EM [63] or AFM [37]. The length distribution, in conjunction with mass per length measurements [66] or the general geometry of the fibrils (width, height [37]), can then be used to estimate the average number of monomers per fibril, which allows to convert the fibril concentration from monomer equivalents to a particle concentration.

When data from ensemble measurements of amyloid fibril growth are analysed in this way, a degree of uncertainty remains even if the macroscopic rates and the relevant concentrations are well defined. This is because it

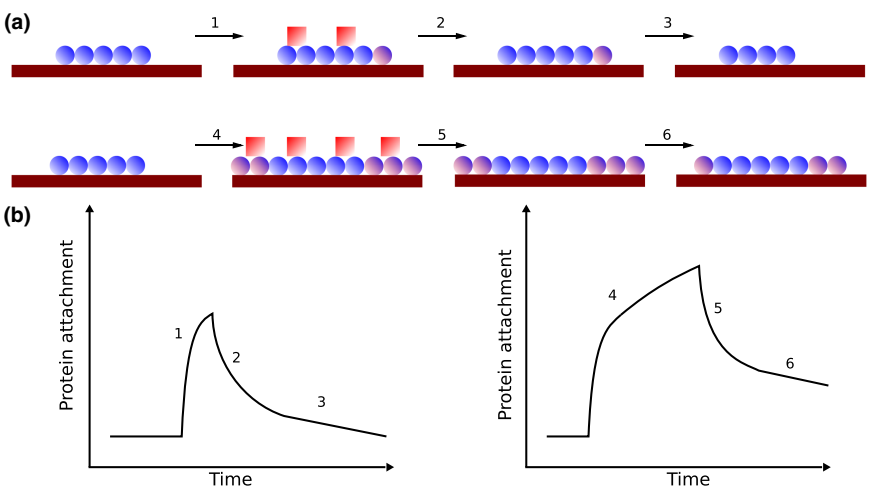

Fig. 4. Surface-based biosensing experiments to distinguish fibril growth from protein attachment to the fibril surface. (**a**) Illustration of a surface-based amyloid fibril growth experiment. (1) short incubation with monomer solution, (2) short buffer wash, (3) long buffer wash. (4) long incubation with monomer, (5) short buffer wash and (6) long buffer wash. (**b**) Illustration of the expected data from the experiments in (**a**), shown for the example of a SPR experiment. Long incubation with monomer yields biphasic behaviour (surface attachment, followed by growth) and long buffer wash also displays biphasic behaviour (surface detachment followed by fibril dissociation).

Biochemical Journal (2019) **476** 2677–2703
https://doi.org/10.1042/BCJ20160868

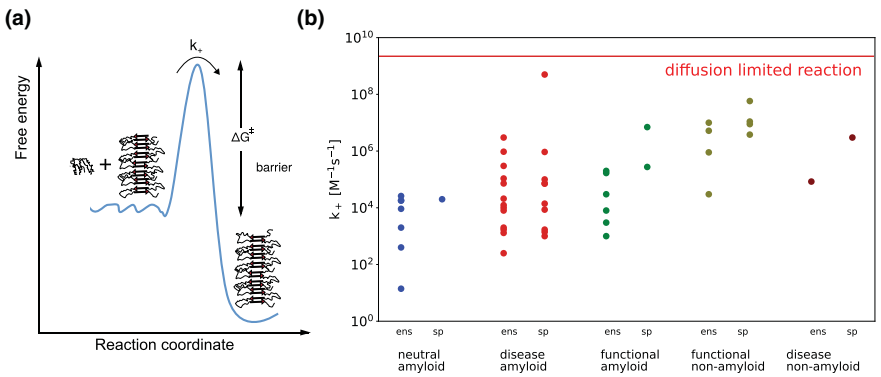

Figure 5. The rate constants of the fibril growth reaction.

(**a**) Despite the fact that the process of amyloid fibril growth might involve the crossing of multiple barriers, the highest barrier determines the absolute rate and hence the process can be approximated as a single barrier crossing event. (**b**) Overview of rate constants of amyloid fibril growth, as well as for the growth of some non-amyloid protein polymers from the literature. An overview of the data is given in Table A2. The data points are separated by the type of amyloid system (disease-related, functional or neutral) and by the measurement technique into ensemble (ens) or single particle (sp) measurements. Neutral amyloid refers to amyloid fibrils that are neither associated with disease, nor with a distinct biological function.

cannot be determined from bulk experiments whether growth occurs at both ends of the fibril or whether it is unidirectional. Different degrees of polarisation of the growth rate have been observed for a range of functional protein polymers [46,67,68], and it is usually explained by the fact that the two ends of a fibril are structurally distinct, which is ultimately due to the asymmetry of the monomeric building blocks. In the case of amyloid fibrils, single particle measurements have revealed that fibril growth is generally polarised, with different degrees of growth rate asymmetry being observed [24,26,28,69–71]. This is particularly straightforward to detect in cases where the seed fibrils and monomeric protein are labelled with different fluorophores and the newly grown parts on both ends can be quantified by a high-resolution optical microscopy [70,71]. A marked difference in growth rate of the two ends reflects a difference in the free energy barrier for monomer addition to the two ends. However, the equilibrium monomer concentration of both ends is obviously identical, and therefore the ratio of on- and off-rate constants is identical for both ends (see Appendix 2). This implies that the end with the faster rate of monomer addition will also have the faster dissociation rate. The highly resolved structural information of amyloid fibrils that is becoming increasingly available from solid-state NMR [72] and cryo-EM [8,9] measurements is likely to aid in rationalising the polarisation of amyloid fibril growth rates. In single particle kinetic studies, it is also often observed that individual fibrils can display widely varying absolute growth rates [69,70] and this observation has been interpreted as a manifestation of the strain phenomenon, i.e. the presence of populations of amyloid fibrils with distinct structures in the sample [69]. The existence of multiple distinct populations of fibrils in a given sample has also been demonstrated unambiguously with the help of cryo-EM [5,6].

Inspection of Figure 5 reveals that the range of measured rate constants of amyloid fibril elongation spans approximately five orders of magnitude (not considering one single particle measurement reporting two orders of magnitude faster rates than any other experiment [65], the inclusion of which leads to a range of more than seven orders of magnitude). In this context, it is interesting to consider the theoretical upper limit of the rate constant of protein polymer growth, which is given by the diffusional arrival of monomeric protein at the polymer end. For a typical protein, a rate constant of $1.8 \times 10^{-9}\ M^{-1}\ s^{-1}$ is obtained (see Appendix 3). This limit is indicated in Figure 5 with a red horizontal line. Therefore, all existing measurements/estimates of amyloid fibril elongation rate constants are below this theoretical limit, even the unusually high estimate from [65]. This means that in all cases, in order for a monomer to incorporate into an amyloid fibril, it will have to cross a (free) energy barrier (see below). The wide range of reported elongation rate constants, therefore, reflects the wide range of the magnitudes of the free energy barriers. The lowest reported rate constants probably do not represent a lower limit of amyloid fibril growth, but rather reflect limitations in the experimental study of very slowly growing amyloid fibrils.

A closer look into Table A2 in Appendix 3 reveals that even for one given peptide, the reported rate constants can differ significantly, often caused by the differences in solution conditions, most notably temperature,

Biochemical Journal (2019) 476 2677–2703
https://doi.org/10.1042/BCJ20160868

pH and ionic strength (see below). This finding highlights an important difference between the growth of amyloid fibrils and that of other types of protein polymers. It can be seen that the functional protein polymers have very similar, relatively high rate constants for growth. This probably reflects partly measurement bias, given that the functional polymers are usually studied under physiological solution conditions, whereas amyloid fibril formation is studied within a much larger region of the space of solution conditions. Nevertheless, the rate constants of amyloid fibril growth appear to be considerably more variable, both between different proteins and for any given protein. The latter feature expresses what might be termed the tunability of amyloid fibril growth rate constants. Qualitatively, the phenomenon of amyloid fibril growth is highly robust against variations in solution conditions, whereas the rate constants can be changed considerably by such variations. Similarly dramatic changes in solution conditions, as those common in the study of amyloid fibrils, would most likely not be tolerated by the proteins forming functional polymers. The latter often polymerise in their native forms and once the native form is destabilised too much such that its structural integrity is compromised, the polymer can no longer form [73].

The energy barriers of amyloid fibril growth

The determination of the rate constant of amyloid fibril growth under any given set of conditions requires, as outlined above, the precise determination of the rate of growth, as well as the concentration of monomeric protein for single particle measurements and in the case of ensemble measurements, the concentration of growing ends needs to be estimated in addition. These parameters, in combination with the assumption that the fibril behaves like a linear polymer [74] allows us to determine the rate constant. Interestingly, the analysis of protein polymer growth rates within the framework of the linear polymerisation model has recently been challenged in the case of tubulin [75] and sickle haemoglobin (HbS) [76], both of which are not truly one-dimensional polymers, and which can also be analysed in the framework of more complex, two-dimensional models. The increasingly detailed structural information available for amyloid fibrils, which reveals that the cross-section of amyloid fibrils mostly consists of more than one monomer and that a single monomer can span several layers of a filament (Figure 1b), may lead to a reconsideration of the applicability of the simple linear polymerisation model to amyloid fibrils. At present, however, it is the model of choice and widely accepted and employed.

In order to determine the (free) energy barriers of amyloid fibril growth, however, an additional layer of modelling is required, which is less firmly established. The basic idea is that the rate constant is a product of two factors, a so-called kinetic pre-factor, Γ, and a Boltzmann factor (exponential factor of a (free) energy):

$$k = \Gamma\, e^{-\Delta G^{\ddagger}/RT}. \tag{1}$$

This functional form expresses the idea that the absolute rate constant consists of the product of an attempt rate to overcome an energy barrier, multiplied with the probability that the molecule has enough energy to actually be able to overcome the barrier. The nature of both of these factors has been, and still is, open for debate. Here, I will not discuss the various possible choices for the nature of the pre-factor and of the energy function in the Boltzmann factor. I will use here the framework whereby the pre-factor is diffusive and the Boltzmann factor contains a free energy barrier, $\Delta G^{\ddagger}$ [48,49]. It is obvious, however, that independently of the actual choice of model, the choice of the pre-factor will influence the numerical value of the barrier. Therefore, if free energy barriers are to be quoted, the numerical values are only meaningful within the context of the pre-factors that were used for their computation. In a previous study, we have presented a model, whereby the pre-factor reflected the overall diffusive motion of the incorporating monomer, as well as the diffusion of the internal degrees of freedom of the polypeptide [48]. However, an even simpler and very instructive choice of diffusional pre-factor is the upper limit for a diffusion-limited reaction presented in the previous section, $\Gamma = k_{max} = 1.8 \times 10^{-9}\ \mathrm{M^{-1}\ s^{-1}}$. The free energy barrier can then simply be computed as:

$$(2)\Delta G^{\ddagger} = RT \log\left(\frac{k_{max}}{k}\right) \tag{2}$$

If, for simplicity, the same pre-factor is used for all the proteins of which data are shown in Figure 5, the magnitude of the free energy barriers can be computed to vary between 13.7 (3.2 if the result from [65] is included) and 46.3 kJ/mol, more than a factor of three (see red boxes in Figure 6a). An important point to consider is

Biochemical Journal (2019) **476** 2677–2703
https://doi.org/10.1042/BCJ20160868

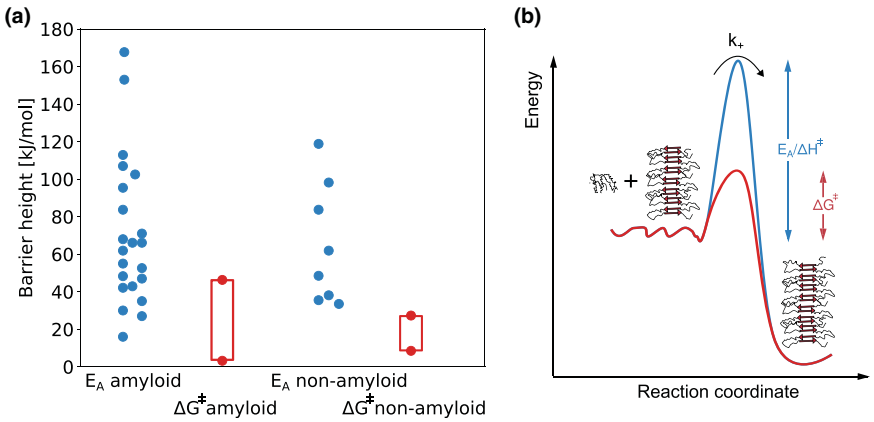

Figure 6. The energy barriers of (amyloid) fibril growth.

(**a**) Plot of Arrhenius activation energies of amyloid fibril growth and of functional protein polymerisation, as well as the corresponding free energy barriers. The latter are given as an energy range with the boundaries defined by the highest and lowest measured values. (**b**) Schematic energy landscape, illustrating that the enthalpic contribution to the free energy barrier is, in most cases, significantly larger than the free energy barrier for both functional and amyloid protein filaments, implying a favourable entropy of activation, which is most likely due to desolvation in the transition state ensemble [49].

that self-assembly of particles with internal degrees of freedom into ordered structures, such as amyloid fibrils, requires a non-vanishing energy barrier. The complete absence of a barrier would signify that every single collision of a monomer with an aggregate is successful, i.e. leads to the addition of the monomer, independently of the place of impact and the orientation and conformation of the impacting monomer, which would most likely lead to the formation of amorphous structures, as is observed under some conditions of salting out of proteins.

At this point, it needs to be discussed how this type of analysis is affected by the finding, in most single particle experiments, that amyloid fibrils are not growing continuously, but rather in a manner that has been termed 'stop-and-go'. This means that if individual fibrils are monitored, periods of growth are interrupted by periods during which the fibrils do not show any sign of growth. In most studies reported to date that have found such stop-and-go behaviour, the durations of the stop and the growth periods are approximately equal. Therefore, if bulk experiments are analysed, the absolute growth rates can be under-estimated by approximately a factor of two. If in addition, the finding is included that amyloid fibril growth can be highly polarised, i.e. most of the growth occurs on one end only, a further factor of two under-estimation can arise if bulk experiments are interpreted such that all fibrils grow all the time with equal rates from both ends. An underestimated absolute growth rate of a factor of four corresponds to an error in the free energy barrier of 3.4 kJ/mol, which is a relatively small (albeit non-negligible) correction on the scale of the absolute values of $\Delta G^{\ddagger}$. Therefore, the main insight stemming from single particle measurements is not necessarily the finding that the absolute growth rates and therefore rate constants can be somewhat higher than those determined from ensemble measurements, but rather the additional insights into the free energy landscape of amyloid fibril growth that can be gained. Given the many independent reports, it is probably safe to assume that the stop-and-go behaviour is a real (albeit not universal [29]) feature of amyloid fibril growth and not a measurement artefact stemming from the fact that most of the single particle experiments are performed with fibrils attached to a surface (which might interfere with the growth). It can, therefore, be deduced from these results that the fibril end can adopt a conformation during the stop phase that is not amenable to the recruitment of new monomers. The considerable lifetimes observed of such states (minutes) suggest that they are relatively stable, similar, in fact, to the 'correct' state which is able to act as a template. At the same time, the probability to access such a state is much lower (one to two orders of magnitude) than that of a correct incorporation. This can be deduced from the observation that during the individual growth phases, dozens to hundreds of monomers adopt the seeding-competent state. It is, therefore, hundreds of times more likely to cross the barrier towards the correctly incorporated, seeding competent state compared with crossing the barrier towards the seeding-incompetent state.

The presence of one, or several, such states is clearly a feature that is not represented if fibril growth is regarded as a single barrier crossing [49]. The existence of such states that are similar in energy to the correctly

Biochemical Journal (2019) 476 2677–2703
https://doi.org/10.1042/BCJ20160868

incorporated state, but unable to recruit more monomers is not surprising. Contrary to the situation in protein folding and functional protein polymer growth, which have experienced evolutionary pressure to become smooth and guide the polypeptide reliably into the correct state, the free energy landscape of amyloid fibril growth cannot be expected to be 'funnel-like' with a well-defined, single minimum. States which are slightly out of register with respect to the templating fibril will be able to form a comparable number of favourable interactions as the correctly incorporated state, but at the same time present a less ideal template for the subsequent monomer. In fact, the very high efficiency of templating of the fibril end in the correct state is one of the most remarkable features of amyloid fibrils. Indeed, the templating effect can be so efficient that a monomer preferably will incorporate into a fibril with a molecular structure different from the one that the monomer would adopt if it were to form fibrils *de novo* under these solution conditions. This finding, which is also known under the term of strain propagation/conservation (as mentioned above, different fibril structures formed by the same amino acid sequence are known as strains), has been confirmed for several proteins and can be explained by the fact that the energy barrier for the nucleation of a new fibril is considerably higher than that for addition onto an existing fibril, even if the latter corresponds to a somewhat sub-ideal template under a given set of conditions.

Having discussed how the free energy barriers of fibril elongation can be computed, I now turn to the question what defines the height of this barrier. Amyloid fibril growth corresponds in all known cases to a dramatic change in the secondary and tertiary structure of the monomer that is incorporating into the fibril, either from intrinsically disordered [77], molten globule [78] or from a wide variety of native or native-like states [79] to β-sheet rich. Importantly, it is not required that the pre-cursor state be unfolded for it to be able to elongate a fibril under any given set of condition. This is, for example, illustrated by early findings during the study of what is now known to be insulin amyloid fibrils [80], which were shown to grow under conditions, such as very low temperatures, where no unfolding of the basic unit (insulin dimer in this case) is detected. A contrasting result has been recently presented, where it has been found that the population of the native state of the PrP correlates negatively with the fibril elongation rate and this has been interpreted as inhibition of the elongation process by the native state. It is possible that in this case, folded and unfolded protein have a similar affinity for the fibril end, but that the probability of correct incorporation (i.e. the height of the main free energy barrier) is significantly lower for the unfolded protein. Before being able to definitively conclude on such an explanation, however, it is important to ascertain that the folded protein does not have an alternative (ThT invisible) reaction pathway available that would have to be taken into account in order to correctly interpret the data.

While unfolding of the monomeric precursor is not required in many cases, solution conditions (pH, temperature, denaturant, see section below), or sequence modifications [81] that destabilise the secondary and tertiary structure of the precursor will generally accelerate amyloid fibril growth. This is, as was pointed out already above, in contrast with the behaviour of biological polymers that form from native, or native-like states, such as actin, tubulin or sickle HbS. Given that ultimately the protein has to radically change structure in order to incorporate into the amyloid fibril, it is plausible to attribute at least part of the free energy barrier to a partial unfolding of the precursor. It is very likely, however, that this partial unfolding is not an isolated event in solution, but rather aided by the fibril end. This implies that the transition state for amyloid fibril growth, the top of the highest free energy barrier separating free monomer from incorporated monomer, corresponds to a structure in which the monomer engages in contact with the fibril end. Strong evidence for this argument comes from different lines of thought, not least the decomposition of the free energy barriers into enthalpic and entropic contributions discussed below. Another argument for an inter-molecular transition state is the polarised growth of amyloid fibrils. If the rate-determining step of the growth reaction were a purely intramolecular (partial unfolding) event, then the interaction with the fibril should not matter, and hence both ends of the fibril would be expected to grow with the same rate.

If the partial unfolding of the native structure of the pre-cursor protein, however, were the only substantial contribution to the free energy barrier, then amyloid fibril growth from intrinsically disordered precursors should be nearly barrier-less. While it is found that some disordered peptides, such as the amyloid β-peptide, indeed display a small free energy barrier for fibril growth, others, such as α-synuclein, display a much more substantial free energy barrier. There is an obvious electrostatic contribution to the barrier, given that in a homo-molecular polymerisation reaction, such as amyloid fibril growth, each of the building blocks carries the same net charge and hence there will be a repulsion between the approaching monomer and the fibril. This contribution to the barrier is independent of the structure of the precursor and will, therefore, also play an

Biochemical Journal (2019) 476 2677–2703
https://doi.org/10.1042/BCJ20160868

important role in the case of unfolded proteins. The contribution of electrostatic repulsion to the free energy barrier can be estimated from experiments at different ionic strength [14], as well as by cross-seeding experiments with protein variants with reduced or increased charge. A further important contribution is likely to stem from the (partial) desolvation of the monomer and fibril end in the transition state, as will be illustrated below.

Having established the magnitudes, and to some extent the origin, of the free energy barriers, the next step in the analysis is to decompose the free energy barriers into their enthalpic and entropic contributions. The method of choice for the decomposition of free energies into the component enthalpic and entropic contributions is a temperature variation. In the case of equilibrium free energies, this method is known as van't Hoff analysis, whereas the analysis of the temperature variation of the kinetics was pioneered by Arrhenius [82]. In Appendix 4, it is shown how a variation in temperature allows us to define the Arrhenius activation energy of amyloid fibril growth, and how this activation energy is linked to the enthalpic contribution to the free energy barrier. For reactions in solution, these two quantities are approximately equal. An important and convenient feature of this analysis is that only the relative change in fibril growth rate with temperature needs to be measured, rather than the absolute rate. In addition, the choice of the kinetic pre-factor, which is intrically linked with the definition of the free energy barrier, only weakly influences the height of the enthalpic barrier. Therefore, the enthalpic barrier is a less model-dependent, more robust quantity compared with the free energy barrier. Also in Appendix 4, many enthalpic barriers for amyloid fibril growth are listed and also, for comparison, enthalpic barriers of some non-amyloid protein polymers.

Comparing the different enthalpic barriers for different proteins and solution conditions, it can be noted that the absolute differences between different proteins are much larger than in the case of the free energy barriers. Interestingly, for those systems where the enthalpic barrier has been measured for the same protein system in different studies, the general agreement between the measurements is good, probably reflecting the simplicity and robustness of the data analysis required to obtain these values.

A remarkable feature that clearly distinguishes amyloid fibril growth from non-amyloid protein polymer growth is the very large temperature range over which the former can be observed, spanning approximately the full temperature range of liquid water. This is in stark contrast with the polymerisation of functional proteins, such as actin, tubulin or flagellin, which form functional polymers only in proximity to normal physiological temperatures (with the exception, perhaps, of functional polymers of extremophiles). As mentioned before, this difference reflects the fundamental feature that proteins need to undergo a substantial structural rearrangement in order to be able to incorporate into an amyloid fibril, whereas functional protein polymers form from native or native-like states that are vulnerable with respect to strong temperature variations. In a previous study, we have discussed the possible determinants of the magnitude of the enthalpy of activation of amyloid fibril growth [49]. We have shown that the magnitude of the barriers correlates both with the size of the protein and with the degree of residual structure in the monomer under the conditions where amyloid fibril growth is studied. The number of new data sets that have been reported since this analysis has been performed is such that a new analysis is not warranted. Indeed, recent reports on the enthalpic barriers for individual proteins, such as Aβ [63,71] or α-synuclein [37] agree well with previous reports [49].

The entropic contribution to the free energy barrier can be simply computed as the difference between the free energy and enthalpy barriers. Of course, the entropy of activation will, therefore, depend as much on the choice of the numerical pre-factor as the free energy, and the numerical values of the entropies of activation contain the combined uncertainties of both the free energy and enthalpy. While, therefore, the absolute values of this quantity might not be very reliable, it is interesting to consider the sign. It was found in the large majority of cases where such an analysis had been performed (amyloid and functional protein polymers, Figure 6a), that the enthalpy of activation is unfavourable and much larger in magnitude than the effective free energy barrier [22,49,83] (Figure 6a,b). Therefore, the entropy of activation can be deduced to be favourable in most cases of filamentous protein aggregation, including amyloid and non-amyloid filaments. The overall energetic signature of the transition state of protein filament growth is, therefore, found to be independent of the exact nature of filament.

We have suggested previously that the origin of the favourable entropic contribution to the free energy barrier of amyloid fibril growth could stem from the hydrophobic effect, i.e. partial desolvation of hydrophobic sequence patches when the incoming protein monomer engages with the fibril end in the transition state. This argument is supported by a correlation (albeit weak) between the average sequence hydrophobicity and the magnitude of the entropic barriers [49]. Such a correlation is expected to be weak at best, given that the large

entropic contribution from the peptide backbone is not taken into account here. The finding that the hydrophobic effect plays a role in the transition state of both amyloid fibril and functional protein polymer growth provides strong evidence for the fact that the highest free energy barrier that has to be crossed by a monomer about to incorporate into a fibril corresponds to a state whereby the monomer is already closely engaged with the fibril end. This model has recently been corroborated by a study that demonstrated that the electrostatic repulsion between the incorporating monomer and the fibril end is very similar in the transition state and the fully incorporated state, also suggesting a close contact between the newly adding monomer and the fibril end in the transition state [84].

Modulation of the amyloid fibril elongation rate by the solution conditions

As mentioned above, the rate constants of amyloid fibril elongation are strongly dependent on the solution conditions and highly tunable. We have discussed the effects of individual factors, such as solution ionic strength or denaturant concentration in some detail in a previous review [85]. Any factor that reduces the free energy difference between the monomeric state and the highest point of the free energy barrier will accelerate the rate of amyloid fibril growth. This free energy difference can be lowered by destabilising the monomeric state or by stabilising the transition state. Destabilising the monomeric state, for example through changes in pH [78,80] and addition of denaturant [22,42], will, of course, be particularly effective in the case where amyloid fibril formation proceeds from fully or partly structured pre-cursors. Alternatively, the transition state can be stabilised, e.g. through the addition of salt, which screens the electrostatic repulsion [14]. Another possibility to stabilise the transition state, if the latter is a more compact state than the precursor, which could be the case in the amyloid fibril growth from intrinsically disordered pre-cursors, is through molecular crowding [86]. The excluded volume effects exerted by a large concentration of crowding agents favour more compact states and can hence stabilise compact transition states.

However, it has also been found that conditions that destabilise the monomeric state, most notably increases in denaturant concentration, will eventually also start to destabilise the transition state and the final state of the elongation reaction, i.e. the fibril. This was the interpretation given to the finding that the fibril growth rates of insulin [22] and PrP [42] are non-monotonic functions of the denaturant concentration.

Changes in pH can affect both the energy of the pre-cursor state, due to a change in intra-molecular charge repulsion, and the energy of the transition state through changes in inter-molecular charge repulsion between the monomer and the fibril end. Whereas the intra-molecular charge distribution is important for the former energy, the global charge of the protein mostly defines the latter. It depends on the interplay of these partly counteracting energetic factors whether a given change in pH will accelerate or slow down amyloid fibril growth.

I will also only very briefly mention inhibition of amyloid fibril growth, because in recent years, several excellent reviews on the topic of inhibition of amyloid fibril formation, in general, have been written, e.g. [87]. Suffice it to say that amyloid fibril growth can be inhibited by adding an inhibitor species to the solution that either interacts with the fibril end [88,89] or with the monomeric protein [90]. However, not every molecule that binds to the monomer will be an efficient inhibitor of fibril growth. It has, for example, been shown that camelid nanobodies can interact with monomeric α-synuclein with high affinity, but that even stoichiometric amounts of the nanobody only reduce the fibril growth rate by approximately a factor of two [91]. This weak effect is presumably caused by the fact that the binding epitope is not involved in the formation of the fibril core [92]. In order to achieve efficient inhibition of fibril elongation, the inhibitor should compete with the fibril end for interaction with the sequence regions that are important for the elongation reaction.

Proposition: Definition of a standard for seeding efficiency of an amyloid fibril preparation

Seeded experiments of amyloid fibril formation are an invaluable tool in the study of protein aggregation, not only in mechanistic investigations, as outlined in detail above, but also, in particular, in the quest for inhibitors of amyloid fibril formation. Especially, strongly seeded experiments can be very fast, robust and reproducible. While such assays are not able to provide insight into whether or not a given inhibitor candidate is able to interfere with any of the nucleation processes, they can be very sensitive towards the detection of interactions between the inhibitor and both the monomer and the fibril ends. The ability to detect very subtle changes in

Biochemical Journal (2019) 476 2677–2703
https://doi.org/10.1042/BCJ20160868

relative elongation rates in appropriately designed seeded assays translates into the detection of even weak interactions between the candidate inhibitor and either the monomer or the fibril end. Conversely, the absence of any detectable inhibitory effect in fibril elongation assays makes a direct interaction between the inhibitor and the monomer unlikely [93]. Lead compounds from such a screen can then be further optimised and also tested in assays that probe for processes other than fibril growth.

One challenge that is being faced when designing and carrying out such screens is to be able to compare data acquired with different batches of seed fibrils. Differences between the behaviour of different seed batches stem most likely from differences in the absolute number of growth competent fibril ends, reflecting, for example, different length distributions or different degrees of higher order assembly of the seed fibrils [37]. Here, I propose a way to formalise such a comparison which, I hope, will contribute to a quantitative and systematic analysis of seeded experiments of amyloid fibril formation. As pointed out above, and outlined in Appendix 1, the strongest criterion for the decision as to whether a certain set of conditions (seed and monomer concentration, solution conditions) is such that only fibril elongation contributes significantly to the data is to test whether or not the data can be well described by single exponential functions. I propose that in assays of amyloid fibril elongation, the conditions should be adjusted in such a way that this is the case, which requires often relatively high seed concentrations of several % by monomer equivalents. At the same time, the reaction should not be too fast, i.e. the time between the addition of the seeds and the start of the measurement should represent a small fraction (∼1%) of the time required to reach the plateau, i.e. to reach equilibrium. The latter condition becomes particularly relevant if many compounds are to be tested and hence many simultaneous reactions are to be prepared. Sequential preparation of the samples translates into different times the individual samples had to react, which compromises direct comparability.

The preparation of a multiwell-plate takes between seconds to minutes, which translates into a recommended characteristic time scale for aggregation of hours. I, therefore, propose that if a given seed concentration leads to a kinetic curve that can be described by a single exponential function with exponential constant $t_s = 1/k_{+,eff} = 1/(k_+P(0)) = 1$ h, then this seed concentration has a seeding efficiency of 1 seeding unit (su). The seeding efficiency of a given seed preparation depends, through the implicit dependence of k_+, on the solution conditions. Therefore, the comparison of two different seed preparations in this manner is only meaningful if both preparations are tested under identical solution conditions and ideally also the same initial monomer concentration.

If, in some large scale screen, different batches of seed fibrils are used, their respective concentrations (as monomer equivalents) can be adjusted such that they will display the same seeding efficiency, greatly facilitating comparison of the data throughout the entire screen.

Summary: the mechanism of amyloid fibril growth

Despite its apparent simplicity, the free energy landscape for the addition of a protein monomer onto the end of an existing seed fibril is complex, with several local minima. A first, shallow class of minima corresponds to the absorption of the monomer onto the fibril end and fibril surface (Figure 7, state 2). Absorption of the monomer onto the fibril end can lead to elongation, whereas absorption onto the fibril surface can lead, with a much lower probability, to the formation of a new fibril through the secondary nucleation. It is at present unknown whether a surface-absorbed monomer can slide along the fibril towards the fibril end and incorporate into the latter without having to detach first. Once the monomer is adsorbed onto the fibril end, it has essentially three options, in order of decreasing probability. First, it can detach again, which is, by far, the most likely event under most conditions. Second, and aided by the fibril end ('templating') it can overcome the barrier for correct incorporation, leading to the energetically most favourable state (for any given template structure). Importantly, this implies an inter-molecular transition state for amyloid fibril growth, whereby the monomer is in close contact with the fibril end. And third, it can overcome other barriers (in Figure 7b, a single one is illustrated) to reach states which are seeding incompetent (state 3). The energy barrier(s) of this process are higher than that of correct incorporation, but the seeding incompetent states are probably less favourable in free energy than the seeding competent ones. The affinity of the monomer for the fibril during initial absorption, as well as the free energy barriers for both correct and incorrect incorporation are very sensitive to the solution conditions, leading to a substantial variability of amyloid fibril growth rates, both between different proteins and within any given protein. All of the above also usually apply if the seed fibril corresponds to a structure that is not the most favourable or kinetically accessible under the given set of solution conditions. The templating effect of the fibril end is able to guide/force the monomer into its own conformation even if

Biochemical Journal (2019) **476** 2677–2703
https://doi.org/10.1042/BCJ20160868

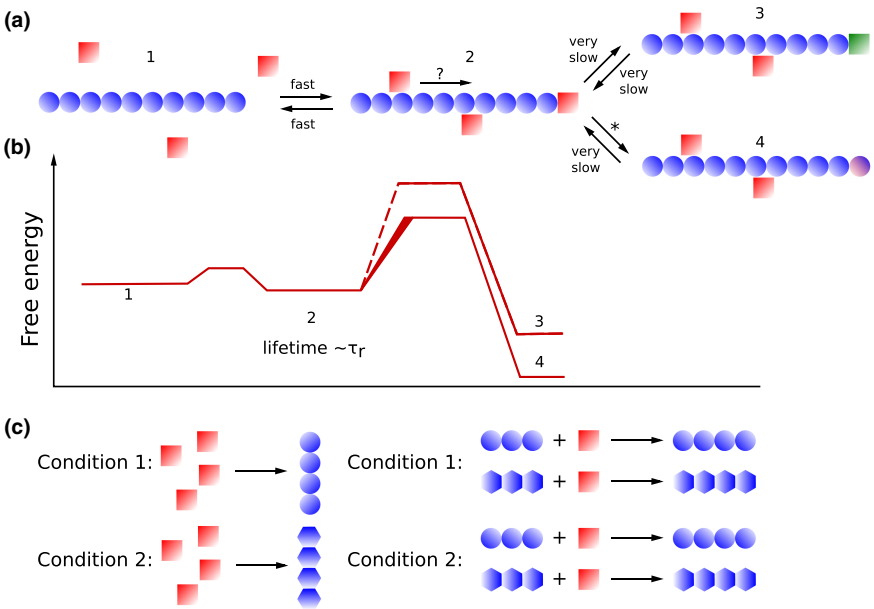

Figure 7. The mechanism of amyloid fibril growth.

(**a**) Illustration of the key states and steps in amyloid fibril growth. (1) Fibril exposed to monomer, (2) monomer weakly absorbed onto fibril surface and fibril end, (3) monomer incorporated incorrectly, seeding incompetent state, (4) monomer incorporated correctly; seeding competent state. (**b**) Relative free energies of the different states. The lifetime of state 2 corresponds approximately to the residency time, τ_r. The transition from state 2 to 4 (marked with an asterisk) is highly variable in its rate, which is reflected in the wide range of observed values for k_+ (Figure 5), even though the experimentally determined values of k_+ contain also contributions from the transitions between states 1 and 2. (**c**) The templating effect of seed fibrils usually overcomes structural preferences imposed by the external solution conditions. This means that the monomer that adds onto the fibril end adopts the conformation imposed by the template rather than the most favourable or accessible fibril structure that is adopted when fibrils form *de novo* under the given solution conditions.

fibrils formed *de novo* under these solution conditions would form a different strain, i.e. adopt a different molecular structure (Figure 7c).

A note of caution is appropriate here: while it can be helpful to picture amyloid fibril growth as a series of discrete steps, it is important to keep in mind that the overall process is best described as a diffusive search for favourable energy states on a free energy landscape [48,94] and it depends on the depth and width of the individual minima how well defined the states along the pathway are.

Open questions

As outlined in this article, much progress has been made in the quantitative understanding of amyloid fibril growth rates. However, some important aspects remain unresolved and will present challenges for research in the years to come. The stunning progress, made in recent years in the determination of amyloid fibril structures at atomic detail, will aid these efforts tremendously.

1. The mechanisms of amyloid fibril growth on a residue-by-residue level are still unresolved. The aim should be to achieve a similar level of understanding to what has been achieved in protein folding [95]. Such studies should be able to take substantial advantage of available fibril structures, and will involve accurate determinations of fibril growth and dissociation rates of sequence variants of a given protein.
2. Most experiments to date have focused on the sensitivity of the overall elongation rate on solution conditions, and little is known about how the different minima and barriers (Figure 7) are influenced by such variations. Such studies require systematic single particle experiments under different sets of conditions (concentration, pH, ionic strength), along the lines of the analysis performed in [71] for changes in temperature.
3. The available structural information also increasingly challenges the picture of amyloid fibrils as truly one-dimensional polymers, i.e. it is found that each monomer inside a fully formed fibril interacts with more

Biochemical Journal (2019) 476 2677–2703
https://doi.org/10.1042/BCJ20160868

than its two nearest neighbours (Figure 1). One likely consequence of such deviations from ideally one-dimensional behaviour are cooperativity effects in the simultaneous parallel growth of several filaments.

4. Relatively few quantitative studies on the relationship between amino acid sequence and the ability to copolymerise have been undertaken [96–99]. The co-aggregation of proteins, of which cross-elongation is only a special case, is the focus of an increasing number of studies and reviews [100,101]. Proteins that are very different in amino acid sequence are unlikely to be able to cross-elongate fibrils. The effects of particular, even small, changes in amino acid sequence on the rates of cross-seeding cannot be currently quantitatively predicted. Qualitatively, it has been established, for example, that decreases in net charge will generally accelerate the growth rates, but the exact effect of any given change in amino acid sequence on the ability to, and rate of, cross-elongation will require structural information of the fibril to be included. Integrated structural and kinetic approaches will lead to more precise definitions of such concepts as 'gate-keeper charges' and have the potential to substantially improve available prediction algorithms.
5. It is intriguing that amyloid fibril growth on surfaces, in particular on lipid bilayers, can display a substantially lower critical concentration compared with that of bulk experiments. It will be insightful to compare surface growth with bulk growth in more detail with the aim to better define the role of the lipid molecules. Closely related to this point is the question as to the differences and similarities of amyloid fibril growth in the test tube and *in vivo*. Among the factors that are known to differ between these conditions, the high surface-to-volume ratio and the omnipresence of lipid bilayers *in vivo* is certainly one of the most relevant ones. Progress in high-resolution optical microscopy has allowed first steps in this direction [102,103] and promises to be translated into new insight in this respect in the near future.

Appendix 1: Elongation-dominated kinetics

The treatment presented here follows closely the one we have outlined before in [37]. In the limit of strong seeding, where other processes, such as primary nucleation, can be neglected, and under quiescent conditions, where fragmentation of fibrils is negligible, the differential equation for the consumption of soluble monomer is given by

$$\frac{\mathrm{d}m(t)}{\mathrm{d}t} = -k_+ P(t) m(t), \tag{A1}$$

where $m(t)$ denotes the monomer concentration at time t, k_+ the molecular rate constant of fibril elongation, and $P(t)$ the number concentration of fibrils (or rather growth-competent ends). Importantly, the dissociation of fibrils is also neglected in this case. If $P(t) = \text{const} = P(0)$ (negligible primary and secondary processes), this equation can be simplified to

$$\frac{\mathrm{d}m(t)}{\mathrm{d}t} = -k_{+,\mathrm{eff}} m(t), \tag{A2}$$

where $k_{+,\mathrm{eff}} = k_+ P(0)$. In the simplest possible representation of amyloid fibril growth as linear polymerisation, there is only one rate constant k_+. However, it is becoming increasingly clear that amyloid fibrils are not truly one-dimensional polymers, as each monomer interacts often with more than two other monomers, at least in mature fibrils. It is, therefore, possible that monomers can occupy non-equivalent positions at the end of the fibril, which implies, in turn, that there could be several different rate constants for monomer addition. However, it is impossible, with current technology, to observe the growth of individual fibrils at sufficient resolution and hence in both single particle and ensemble experiments, the fibril(s) grow(s) with an effective rate constant. Therefore, the above equation is a valid description of fibril elongation experiments even if linear polymerisation is a simplification.

The solution to this equation with the initial monomer concentration $m(0)$ is given by $m(t) = m(0)\,\mathrm{e}^{-k_{+,\mathrm{eff}} t}$, from where it can be seen that (due to the neglecting of fibril dissociation), the monomer concentration decreases exponentially to zero. Often, the increase in fibrillar mass concentration (via an increase in ThT fluorescence) is measured, rather than the decrease in monomer concentration. Therefore, the normalized

Biochemical Journal (2019) 476 2677–2703
https://doi.org/10.1042/BCJ20160868

expression for the observed increase in fibrillar mass $M(t)$, using $M(t) + m(t) = m(0)$ is given by

$$\frac{M(t)}{m(0)} = 1 - e^{-k_{+,\mathrm{eff}}t}. \tag{A3}$$

Here, the contribution to the signal stemming from the mass of the initially present seeds has been neglected. This corresponds to subtraction of the signal present at the start of the experiment. If a given kinetic curve of seeded aggregation can be well described and fitted by this expression, this provides strong evidence that all molecular processes other than fibril growth can be neglected. Under these conditions, I define $t_s = 1/k_{+,\mathrm{eff}} = 1\,\mathrm{h}$ as one seeding unit, SU. This quantity will allow easy comparability between different batches of seed fibrils.

Appendix 2: The concentration-dependence of amyloid fibril elongation

As outlined in Appendix 1, amyloid fibril growth can be described as a reaction between a fibril end and a protein monomer. If the aim is to explore the behaviour at low monomer concentrations, it is no longer possible to neglect the dissociation of fibrils. Therefore, the differential equation for the rate of change of monomer concentration becomes

$$\frac{\mathrm{d}m(t)}{\mathrm{d}t} = -k_+P(t)m(t) + k_-P(t), \tag{A4}$$

where k_- is the dissociation rate constant. Assuming again that the number of fibril ends, $P(t) = P(0) = \mathrm{const.}$ and calling $m(0) = m_0$, the monomer concentration at $t = 0$, the following solution is obtained:

$$m(t) = e^{-P(0)k_+t}\left(m_0 - \frac{k_-}{k_+}\right) + \frac{k_-}{k_+}. \tag{A5}$$

This equation has the equilibrium (long time) solution:

$$m(\infty) = m_{\mathrm{eq}} = m_{\mathrm{crit}} = \frac{k_-}{k_+}. \tag{A6}$$

At equilibrium, therefore:

$$k_+P(0)m_{\mathrm{eq}} = k_-P(0). \tag{A7}$$

At the equilibrium ('critical') concentration, fibril growth and dissociation balance. It can be easily seen from this equation that if $m > m_{\mathrm{eq}}$, there will be net growth and if $m < m_{\mathrm{eq}}$, there will be net dissociation of the fibrils. Therefore, the amyloid fibril growth rate is a linear function of the monomer concentration and zero net growth is reached at a finite monomer concentration.

It has been empirically found that most linear protein polymers display a sub-linear concentration dependence of their growth rates at higher concentrations [39,48,58], i.e. that the growth rate saturates at higher monomer concentrations. The functional behaviour resembles that of Michaelis–Menten kinetics and it was indeed found that an equation of the form:

$$\frac{\mathrm{d}m(t)}{\mathrm{d}t} = -\frac{k_{+,\mathrm{eff}}m_{1/2}m(t)}{m(t) + m_{1/2}} \tag{A8}$$

provides a good description of the data. Here, as before $k_{+,\mathrm{eff}} = k_+P(0)$ and $m_{1/2}$ represents the monomer concentration at which half of the maximally possible fibril elongation rate is reached. This expression has the

Biochemical Journal (2019) 476 2677–2703
https://doi.org/10.1042/BCJ20160868

limits $\lim_{m\to+\infty} \mathrm{d}m(t)/\mathrm{d}t = -k_{+,\mathrm{eff}} m_{1/2} = \mathrm{const}$ and $\lim_{m\to 0} \mathrm{d}m(t)/\mathrm{d}t = -k_{+,\mathrm{eff}} m(t)$.[1] It should be noted that $k_{+,\mathrm{eff}}$ corresponds to $k_{\mathrm{cat}} E_0 / K_{\mathrm{M}}$ of the Michaelis–Menten formalism, and therefore the linear dependence of the fibril elongation rate with monomer concentration with rate constant k_+ ignores the multi-step nature of the growth process and treats it as a single barrier crossing.

This more general expression can also be integrated with m_0 as the monomer concentration at time 0 and yields the following expression:

$$m(t) = m_{1/2} W\left(\frac{e^{m_0/m_{1/2} - k_{+,\mathrm{eff}} t} m_0}{m_{1/2}}\right), \tag{A9}$$

where W denotes the Lambert W (or product log) function, which is defined through the equation $z = W(z)\, e^{W(z)}$ for any $z \in \mathbb{C}$. It has been proposed that the saturating concentration can be extracted directly from a fit of a single aggregation curve to this model [59], rather than from the analysis of the initial rates at a range of different monomer concentrations [39,48].

We have previously shown, using the formalism of diffusive barrier crossing and dimensionality arguments, that the characteristic concentration at which the elongation rate starts to saturate can be linked to a time scale τ_r through [48]:

$$m_{1/2} = \frac{1}{D r_{\mathrm{eff}} \tau_r}, \tag{A10}$$

whereby r_{eff} represents a characteristic length scale. In our previous work, we have used polymer physics to estimate the sequence-length dependence of r_{eff} [48]. Here, I use a simplified treatment, whereby I make use of the fact that the diffusion coefficient can be written as $D = k_B T / 6\pi\eta r$, where r is the radius of the diffusing molecule and η is the viscosity. By equating the size of the molecule with the characteristic dimension of the reactive site at the fibril end, an expression for the time scale τ_r is obtained:

$$\tau_r = \frac{6\pi\eta}{k_B T m_{1/2}}, \tag{A11}$$

τ_r can be thought of as an average residency time of a monomer at the fibril end. While the fibril end is occupied by one monomer that is not yet incorporated into the fibril, further monomers are unable to add onto the fibril. This explains the saturation effect at higher concentration. It is interesting to compare the saturation concentrations and residency times for amyloid fibril formation of different proteins under different conditions. Without any claim of completeness, I have collected such data from the literature, and they are plotted in Figure 3 and the data are listed in Table A1, together with the literature references. The value of $m_{1/2}$ is only directly given in some of the references; in those cases where it is not explicitly stated, I have extracted the data and fitted them to the model discussed above.

It can be seen from Table A1 that the values of $m_{1/2}$ and hence of τ_r can differ considerably, between different proteins, but even for any given protein upon change in sequence or solution conditions. This variability is most clearly illustrated in the case of the PrP, for which it was shown that a change in solution conditions (variation of denaturant concentration) can be used to tune the concentration dependence of fibril growth from very low saturation concentrations of the order of a few μM to hundreds of μm [42]. I conclude, therefore, that the saturation concentration of amyloid fibril elongation is unlikely to represent a characteristic feature of each protein, but rather reflects the magnitude of the weak interactions between the monomer and the fibril end, while the monomer is not yet correctly incorporated into the fibril. The magnitude of these weak interactions is subject to strong relative variations upon changes in solution conditions.

The value of $m_{1/2}$ for flagellin [58] is included in Table A1 as the only example of a functional protein polymer. For actin [68,107] and tubulin [75], only filament growth rates at low concentrations are available. For sickle HbS, the concentrations used in typical experiments are so high (several mM) that the activity

[1]The dissociation of fibrils has been neglected here and therefore the limit of small concentrations should read: $\lim_{m\to m_{\mathrm{eq}}} \mathrm{d}m(t)/\mathrm{d}t = -k_{+,\mathrm{eff}} m(t)$.

Biochemical Journal (2019) 476 2677–2703
https://doi.org/10.1042/BCJ20160868

Table A1. Overview of the values of the saturation concentration of amyloid fibril elongation, $m_{1/2}$, accessible in the current literature, as well as the equivalent residency times, τ_r

Peptide/protein	Number of residues	Temperature (°C)	$m_{1/2}$ (M)	τ_r (s)	References
Insulin	51	70	105.5	2.51×10^{-5}	[104]
Insulin	51	40	499	9.4×10^{-6}	[22]
Insulin	51	40	818	5.8×10^{-5}	[48]
Insulin (+ salt)	51	37	299	1.71×10^{-5}	[59]
Insulin (− salt)	51	37	95	5.39×10^{-5}	[59]
α-synuclein	140	37	46	1.30×10^{-4}	[37]
α-synuclein	140	37	25	2.05×10^{-4}	[105]
α-syn (1–119)	119	37	10	5.12×10^{-4}	[105]
α-syn (1–103)	103	37	11	4.66×10^{-4}	[105]
Sup35	254	25	7	9.78×10^{-4}	[39]
S6	96	42	8	5.58×10^{-4}	[40]
Aβ (1–40)	40	25	59	1.16×10^{-4}	[13]
Aβ (1–40)	40	37	222	2.3×10^{-5}	[106]
Aβ (1–42)	42	25	7.2	9.51×10^{-4}	[71]
tau K18	130	25	37	1.85×10^{-4}	[43]
tau K19	99	25	18	3.81×10^{-4}	[43]
PrP (2.3 M GndHCl)	207	37	18	2.85×10^{-4}	[42]
PrP-V210A (2.3 M GndHCl)	207	37	112	4.57×10^{-5}	[42]
Salmonella flagellin	495	26	96	7.11×10^{-5}	[58]

The temperatures were used to adjust the values of the viscosity η in each case.

coefficient γ differs substantially from unity (values of γ of 10 and more can be reached [108]), rendering it difficult to distinguish saturation effects from activity coefficient-related effects on the net growth rate.

Appendix 3: The rate constants of amyloid fibril growth

Before considering the experimentally determined rate constants for amyloid fibril elongation, it is interesting to recall the maximal possible bi-molecular reaction rate constants in solution. If the reaction consists in the capture of a species A, with diffusion coefficient D_A and concentration c_A by a sphere of Radius R, then the diffusion-limited reaction rate in solution, Φ_{max} is given by [109]:

$$\Phi_{max} = 4\pi D_A R c_A = k_{max} c_A \tag{A12}$$

This situation is a good approximation for the case whereby the elongation reaction consists in the diffusion of a protein monomer into a reaction volume at the fibril end, because the fibril will have a much lower diffusion coefficient than the monomer and hence appears stationary, even in the case where elongation occurs freely in solution. It has to be noted, however, that fibril elongation might also have contributions from monomer that attaches to the fibril surface, then slides along the fibril and incorporates into the fibril end when it reaches the end. This putative contribution to fibril elongation could increase the maximal possible (barrier-less) rate. However, for the simple estimate of the maximally possible, diffusion-limited fibril elongation rate, this aspect can be neglected. The diffusion-limited elongation rate constant is therefore given by

$$k_{max} = 4\pi D R = \frac{4 k_B T}{6\eta}, \tag{A13}$$

Biochemical Journal (2019) **476** 2677–2703
https://doi.org/10.1042/BCJ20160868

Table A2. Rate constants of protein polymer growth Part 1 of 2

Peptide/ protein	Experimental method	Single particle/ ensemble	Temperature (°C)	Rate constant (M^{-1} s^{-1})	Neutral/disease/ functional	References
Glucagon	QCM	Ensemble	25	$1.8 \cdot 10^4$	Neutral	[49]
Glucagon	TIRF	Single particle	21	$2 \cdot 10^4$	Neutral	[110]
Insulin B-chain	QCM	Ensemble	25	$1.8 \cdot 10^4$	Neutral	[49]
Insulin	QCM	Ensemble	25	$4 \cdot 10^2$	Neutral	[49]
Insulin	QCM	Ensemble	∼25	$9.2 \cdot 10^3$	Neutral	[22]
α-lactalbumin	QCM	Ensemble	25	$2.6 \cdot 10^4$	Neutral	[49]
β-lactoglobulin	QCM	Ensemble	25	$1.4 \cdot 10^1$	Neutral	[49]
PI3K-SH3	QCM	Ensemble	25	$2 \cdot 10^3$	Neutral	[49]
Aβ (1–42)	QCM	Ensemble	25	$9.5 \cdot 10^5$	Disease	[49]
Aβ (1–42)	ThT	Ensemble	37	$3 \cdot 10^6$	Disease	[111]
Aβ (1–42)	TIRF	Single particle	∼25	$9.3 \cdot 10^5$	Disease	[71]
Aβ (1–40)	ThT	Ensemble	37	$3 \cdot 10^5$	Disease	[106]
Aβ (1–40)	AFM	Single particle	37	$7.2 \cdot 10^4$	Disease	[112]
Aβ (1–40)	TIRF-QCM	Single particle	25	$5 \cdot 10^8$	Disease	[65]
Aβ (1–40)	AFM	Single particle	24	$1.4 \cdot 10^4$	Disease	[113]
Aβ (1–40)	TIRF	Single particle	37	$1 \cdot 10^5$	Disease	[114]
α-synuclein	QCM	Ensemble	25	$2.1 \cdot 10^4$	Disease	[49]
α-synuclein	dSTORM	Single particle	37	$1 \cdot 10^3$	Disease	[49]
α-synuclein	ThT	Ensemble	37	$2.2 \cdot 10^3$	Disease	[37]
α-synuclein	ThT	Ensemble	37	$1.3 \cdot 10^3$	Disease	[37]
α-synuclein	TIRF	Single particle	25	$8.6 \cdot 10^3$	Disease	[32]
amylin	AFM	Single particle	∼25	$1.7 \cdot 10^3$	Disease	[24]
amylin	TIRF	Single particle	24	$1.4 \cdot 10^3$	Disease	[115]
β2-microglobulin	QCM	Ensemble	25	$8 \cdot 10^3$	Disease	[49]
β2-microglobulin	ThT	Ensemble	25	$7.2 \cdot 10^4$	Disease	[41]
β2-microglobulin	TIRF	Single particle	37	$7.1 \cdot 10^4$	Disease	[116]
lysozyme ox.	QCM	Ensemble	25	$2.5 \cdot 10^2$	Disease	[49]
lysozyme red.	QCM	Ensemble	25	$1.1 \cdot 10^5$	Disease	[49]
$K_2Q_{47}K_2$	Sol. protein	Ensemble	25	$\sim 1 \cdot 10^4$	Disease	[117]
$K_2Q_{23}K_2$	Sol. protein	Ensemble	37	$1.24 \cdot 10^4$	Disease	[118]
$K_2Q_{10}pGQ_{11}K_2$	Sol. protein	Ensemble	37	$1.7 \cdot 10^3$	Disease	[119]
Ure2 Sc	QCM	Ensemble	25	$1.7 \cdot 10^5$	Functional	[49]
Ure2 Sc	ThT	Ensemble	4	$1 \cdot 10^3$*	Functional	[120]
Ure2 Sp	ThT	Ensemble	4	$3 \cdot 10^3$*	Functional	[120]
Sup35	ThT	Ensemble	25	$2 \cdot 10^5$	Functional	[39]
Sup35	AFM	Single particle	∼25	$5 \cdot 10^4 - 5 \cdot 10^5$†	Functional	[69]
CsgA	ThT	Ensemble	37	$3 \cdot 10^4$	Functional	[121]
CsgA	AFM	Single particle	25	$7 \cdot 10^6$	Functional	[122]
FapC	ThT	Ensemble	37	$8 \cdot 10^3$	Functional	[121]
ATP-actin	Pyrene fluo.	Ensemble	25	$1 \cdot 10^7$	Funct. non-amyloid	[123]

Continued

Biochemical Journal (2019) **476** 2677–2703
https://doi.org/10.1042/BCJ20160868

Table A2. Rate constants of protein polymer growth Part 2 of 2

Peptide/ protein	Experimental method	Single particle/ ensemble	Temperature (°C)	Rate constant (M^{-1} s^{-1})	Neutral/disease/ functional	References
ATP-/ADP-actin	EM	Single particle	22	$11/3.8 \cdot 10^6$	Funct. non-amyloid	[68]
ATP-/ADP-actin	Pyrene fluo.	Ensemble	25	$5.2/0.9 \cdot 10^6$	Funct. non-amyloid	[124]
Tubulin	TIRF	Single particle	34	$5.8 \cdot 10^7$	Funct. non-amyloid	[75]
Tubulin	DIC microsc.	Single particle	37	$8.9 \cdot 10^6$	Funct. non-amyloid	[46]
Flagellin	Centrifugation	Single particle	26	$3 \cdot 10^4$	Funct. non-amyloid	[58]
HbS	Las. photolys.	Ensemble	25	$8.4 \cdot 10^4$	Non-amyloid dis.	[108]
HbS	DIC microsc.	Single particle	25	$3 \cdot 10^6$	Non-amyloid dis.	[76]

Listed are mostly values for amyloid fibrils, but for comparison also values for non-amyloid functional and disease-related protein polymers. In some references, the numerical value of k_+ is directly quoted, but in others values for the absolute growth rate are given together with the monomer concentration at which the experiments were performed, which allows to calculate the rate constant.
*Calculated under the assumption that the average number of monomers in the seed fibrils to be 200 (estimated from TEM images of seed fibrils).
†Calculated under the assumption that the fibrils consist of 0.3 monomers/nm (from protein molecular mass and AFM fibril thickness), and reflecting the observed spread in single fibril growth rates.

where I have used the expression for the diffusion coefficient, $D = k_B T/6\pi\eta r$ and I have made the simplifying assumption that the radius r of the protein monomer is approximately equal to the reaction volume R at the fibril end. Therefore, the value for the diffusion-limited rate constant is $k_{\max} = 3.05 \times 10^{-18}\ \mathrm{m^3\ s^{-1}}$, which can be converted into molar units by multiplying with Avogadro's number and converting from m^3 into litre, yielding $k_{\max} = 1.8 \times 10^9\ \mathrm{M^{-1}\ s^{-1}}$.

It is insightful to compare this upper bound to the rate constants actually observed in the measurements of protein polymer growth. I have prepared a collection of literature values for k_+ in Table A2 not only for amyloid fibrils, but also for non-amyloid protein polymers. The rate constants are plotted in Figure 5 of the main manuscript.

Appendix 4: The temperature dependence of amyloid fibril growth rates

In the simple Arrhenius picture, a rate constant consists of the product of a pre-factor A and an exponential factor with an activation energy, E_A:

$$k = Ae^{-E_A/RT}. \tag{A14}$$

If the logarithm of the rate constant is plotted against the inverse temperature, the Arrhenius activation energy, E_A, can be determined:

$$\frac{\mathrm{d}\log(k)}{\mathrm{d}(\frac{1}{T})} = -\frac{E_A}{R}. \tag{A15}$$

Some values of E_A from the literature are listed in Table A3.

Formally, the activation energy is not identical with the activation enthalpy. However, it can be shown that they are numerically very close. The reason why these two quantities differ is that in the Arrhenius theory, the

Biochemical Journal (2019) **476** 2677–2703
https://doi.org/10.1042/BCJ20160868

Table A3. Activation energies for the elongation step of various amyloid systems, as well as some non-amyloid protein polymers

Peptide/protein	E_A (kJ/mol)	References
Glucagon	30.0 ± 12.0	[49]
Insulin B-chain	35.0 ± 10.0	[49]
Insulin	102.5 ± 4.2	[22]
Aβ (1–42)	66.1 ± 8.1	[49]
Ure2p	27.0 ± 10.0	[49]
PI3K-SH3	42.1 ± 8.5	[49]
β2-microglobulin	48.3 ± 8.6	[49]
α-lactalbumin	107.0 ± 10.0	[49]
Lysozyme ox.	167.7 ± 14.7	[49]
Lysozyme red.	68 ± 12	[49]
α-synuclein	71.0 ± 5.6	[49]
α-synuclein	52.6 ± 3.2	[37]
Bovine β-lactoglob.	83.7 ± 9.6	[49]
Aβ (1–40)	95.4 ± 4.6	[83]
Aβ (1–40)	61.9 ± 1.3	[125]
Aβ (1–40)	42.9	[20]
Aβ (1–42)	66.1 ± 8.1	[49]
Aβ (1–42)	55 ± 5	[63]
Aβ (1–42)	47 ± 17	[71]
Het-S	16 ± 2	[126]
Stefin B	112.9 ± 20.9	[127]
Ig light chain	153 ± 12	[128]
ATP-actin	35.5	[107]
ATP-/ADP-actin	83.7/98.2	[129]
ATP-actin	61.9	[130]
Tubulin	33.5	[131]
Tubulin	48.5 ($T > 28°$)	[132]
Tubulin	118.8 ($T < 28°$)	[132]
HbS	38.1 ± 2.5	[108]

kinetic pre-factor is temperature independent, whereas in more modern reaction rate theories, such as transition state theory for gas phase ractions [133], or Kramer's theory for diffusive reactions in solution [134], the pre-factor depends on temperature. Interestingly, in both theories, there is an explicit linear temperature dependence. The Eyring pre-factor is k_BT/h and the Kramers pre-factor contains the diffusion coefficient which depends linearly on $T : D = k_BT/6\pi\eta r$. D also depends in addition on temperature through its dependence on solution viscosity η, which itself is temperature dependent. The Arrhenius equation can therefore be written as

$$\frac{\mathrm{d}\log(k_A)}{\mathrm{d}T} = \frac{E_A}{RT^2} \tag{A16}$$

and for the case of a diffusive reaction in solution, where the rate constant can be written as (due to the

assumption of linear temperature dependence of A):

$$\frac{\mathrm{d}\log(k_D)}{\mathrm{d}T} = \frac{1}{T} + \frac{H^{\ddagger}}{RT^2} \tag{A17}$$

and therefore

$$\frac{E_A}{RT^2} = \frac{1}{T} + \frac{H^{\ddagger}}{RT^2} \tag{A18}$$

and hence $E_A = H^{\ddagger} + RT$. This means that the difference between the Arrhenius activation energy and the enthalpy of activation is ~2.5 kJ/mol, which is smaller than the experimental uncertainties of most of the experimental data, which allows to treat Arrhenius activation energy and enthalpy of activation as being approximately equal.

Abbreviations

CD, circular dichroism (CD); DLS, dynamic light scattering; FRET, Förster resonance energy transfer; HbS, haemoglobin; ITC, isothermal titration calorimetry; NMR, nuclear magnetic resonance; PrP, prion protein; QCM, quartz crystal microbalance; SPR, surface plasmon resonance; ThT, Thioflavin-T.

Acknowledgments

I thank the Novo Nordisk Foundation for support through a Novo Nordisk Foundation professorship and also thank Emil G. P. Stender, Nicola Vettore and Céline Galvagnion for critical reading of the manuscript.

Competing Interests

The Authors declare that there are no competing interests associated with the manuscript.

References

1 Cohen, S.I.A., Vendruscolo, M., Welland, M.E., Dobson, C.M., Terentjev, E.M. and Knowles, T.P.J. (2011) Nucleated polymerization with secondary pathways. I. Time evolution of the principal moments. *J. Chem. Phys.* **135**, 065105https://doi.org/10.1063/1.3608916
2 Buell, A.K. (2017) The nucleation of protein aggregates-from crystals to amyloid fibrils. *Int. Rev. Cell. Mol. Biol.* **329**, 187–226 https://doi.org/10.1016/bs.ircmb.2016.08.014
3 Knowles, T.P.J, Waudby, C.A., Devlin, G.L., Cohen, S.I.A., Aguzzi, A., Vendruscolo, M. et al. (2009) An analytical solution to the kinetics of breakable filament assembly. *Science* **326**, 1533–1537 https://doi.org/10.1126/science.1178250
4 Dobson, C.M. (2003) Protein folding and misfolding. *Nature* **426**, 884–890 https://doi.org/10.1038/nature02261
5 Fitzpatrick, A.W.P., Debelouchina, G.T., Bayro, M.J., Clare, D.K., Caporini, M.A., Bajaj, V.S. et al. (2013) Atomic structure and hierarchical assembly of a cross-β amyloid fibril. *Proc. Natl Acad. Sci. U.S.A.* **110**, 5468–5473 https://doi.org/10.1073/pnas.1219476110
6 Fitzpatrick, A.W.P., Falcon, B., He, S., Murzin, A.G., Murshudov, G., Garringer, H.J. et al. (2017) Cryo-EM structures of tau filaments from Alzheimer's disease. *Nature* **547**, 185–190 https://doi.org/10.1038/nature23002
7 Gremer, L., Schölzel, D., Schenk, C., Reinartz, E., Labahn, J., Ravelli, R.B.G. et al. (2017) Fibril structure of amyloid-β(1-42) by cryo-electron microscopy. *Science* **358**, 116–119 https://doi.org/10.1126/science.aao2825
8 Guerrero-Ferreira, R., Taylor, N.M., Mona, D., Ringler, P., Lauer, M.E., Riek, R. et al. (2018) Cryo-em structure of alpha-synuclein fibrils. *eLife* **7**, e36402 https://doi.org/10.7554/eLife.36402
9 Röder, C., Vettore, N., Mangels, L.N., Gremer, L., Ravelli, R.B., Willbold, D. et al. (2019) Atomic structure of PI3-kinase SH3 amyloid fibrils by cryo-electron microscopy. *Nat. Commun.* **10**, 3754 https://doi.org/10.1038/s41467-019-11320-8
10 Klingstedt, T., Aslund, A., Simon, R.A., Johansson, L.B., Mason, J.J., Nyström, S. et al. (2011) Synthesis of a library of oligothiophenes and their utilization as fluorescent ligands for spectral assignment of protein aggregates. *Org. Biomol. Chem.* **9**, 8356–8370 https://doi.org/10.1039/c1ob05637a
11 Gade Malmos, K, Blancas-Mejia, L.M., Weber, B, Buchner, J, Ramirez-Alvarado, M, Naiki, H et al. (2017) ThT 101: a primer on the use of thioflavin T to investigate amyloid formation. *Amyloid* **24**, 1–16 https://doi.org/10.1080/13506129.2017.1304905
12 Bouchard, M., Zurdo, J., Nettleton, E.J., Dobson, C.M. and Robinson, C.V. (2000) Formation of insulin amyloid fibrils followed by FTIR simultaneously with CD and electron microscopy. *Protein Sci.* **9**, 1960–1967 https://doi.org/10.1110/(ISSN)1469-896X
13 Lomakin, A., Chung, D.S., Benedek, G.B., Kirschner, D.A. and Teplow, D.B. (1996) On the nucleation and growth of amyloid beta-protein fibrils: detection of nuclei and quantitation of rate constants. *Proc. Natl Acad. Sci. U.S.A.* **93**, 1125–1129 https://doi.org/10.1073/pnas.93.3.1125
14 Buell, A.K., Hung, P., Salvatella, X., Welland, M.E., Dobson, C.M. and Knowles, T.P.J. (2013) Electrostatic effects in filamentous protein aggregation. *Biophys. J.* **104**, 1116–1126 https://doi.org/10.1016/j.bpj.2013.01.031
15 Ikenoue, T., Lee, Y.-H., Kardos, J., Yagi, H., Ikegami, T., Naiki, H. et al. (2014) Heat of supersaturation-limited amyloid burst directly monitored by isothermal titration calorimetry. *Proc. Natl Acad. Sci. U.S.A.* **111**, 6654–6659 https://doi.org/10.1073/pnas.1322602111
16 Kardos, J., Yamamoto, K., Hasegawa, K., Naiki, H. and Goto, Y. (2004) Direct measurement of the thermodynamic parameters of amyloid formation by isothermal titration calorimetry. *J. Biol. Chem.* **279**, 55308–55314 https://doi.org/10.1074/jbc.M409677200

Biochemical Journal (2019) **476** 2677–2703
https://doi.org/10.1042/BCJ20160868

17 Jeppesen, M.D., Hein, K., Nissen, P., Westh, P. and Otzen, D.E. (2010) A thermodynamic analysis of fibrillar polymorphism. *Biophys. Chem.* **149**, 40–46 https://doi.org/10.1016/j.bpc.2010.03.016
18 Buell, A.K., White, D.A., Meier, C., Welland, M.E., Knowles, T.P.J. and Dobson, C.M. (2010) Surface attachment of protein fibrils via covalent modification strategies. *J. Phys. Chem. B* **114**, 10925–10938 https://doi.org/10.1021/jp101579n
19 Myszka, D.G., Wood, S.J. and Biere, A.L. (1999) Analysis of fibril elongation using surface plasmon resonance biosensors. *Methods Enzymol.* **309**, 386–402 https://doi.org/10.1016/S0076-6879(99)09027-8
20 Hasegawa, K., Ono, K., Yamada, M. and Naiki, H. (2002) Kinetic modeling and determination of reaction constants of Alzheimer's β-amyloid fibril extension and dissociation using surface plasmon resonance. *Biochemistry* **41**, 13489–13498 https://doi.org/10.1021/bi020369w
21 Cannon, M.J., Williams, A.D., Wetzel, R. and Myszka, D.G. (2004) Kinetic analysis of beta-amyloid fibril elongation. *Anal. Biochem.* **328**, 67–75 https://doi.org/10.1016/j.ab.2004.01.014
22 Knowles, T.P.J., Shu, W., Devlin, G.L., Meehan, S., Auer, S., Dobson, C.M. et al. (2007) Kinetics and thermodynamics of amyloid formation from direct measurements of fluctuations in fibril mass. *Proc. Natl Acad. Sci. U.S.A.* **104**, 10016–10021 https://doi.org/10.1073/pnas.0610659104
23 Kotarek, J.A., Johnson, K.C. and Moss, M.A. (2008) Quartz crystal microbalance analysis of growth kinetics for aggregation intermediates of the amyloid-β protein. *Anal. Biochem.* **378**, 15–24 https://doi.org/10.1016/j.ab.2008.03.022
24 Goldsbury, C., Kistler, J., Aebi, U., Arvinte, T. and Cooper, G.J.S. (1999) Watching amyloid fibrils grow by time-lapse atomic force microscopy. *J. Mol. Biol.* **285**, 33–39 https://doi.org/10.1006/jmbi.1998.2299
25 Hoyer, W., Cherny, D., Subramaniam, V. and Jovin, T.M. (2004) Rapid self-assembly of α-synuclein observed by in situ atomic force microscopy. *J. Mol. Biol.* **340**, 127–139 https://doi.org/10.1016/j.jmb.2004.04.051
26 Kellermayer, M.S.Z., Karsai, A., Benke, M., Soos, K. and Penke, B. (2008) Stepwise dynamics of epitaxially growing single amyloid fibrils. *Proc. Natl Acad. Sci. U.S.A.* **105**, 141–144 https://doi.org/10.1073/pnas.0704305105
27 Milhiet, P.-E., Yamamoto, D., Berthoumieu, O., Dosset, P., Grimellec, C.L., Verdier, J.-M. et al. (2010) Deciphering the structure, growth and assembly of amyloid-like fibrils using high-speed atomic force microscopy. *PLoS ONE* **5**, e13240 https://doi.org/10.1371/journal.pone.0013240
28 Watanabe-Nakayama, T., Ono, K., Itami, M., Takahashi, R., Teplow, D.B. and Yamada, M. (2016) High-speed atomic force microscopy reveals structural dynamics of amyloid β 1-42 aggregates. *Proc. Natl Acad. Sci. U.S.A.* **113**, 5835–5840 https://doi.org/10.1073/pnas.1524807113
29 Xu, Y., Safari, M.S., Ma, W., Schafer, N.P., Wolynes, P.G. and Vekilov, P.G. (2019) Steady, Symmetric, and Reversible Growth and Dissolution of Individual Amyloid-β Fibrils. *ACS Chem. Neurosci.* **10**, 2967–2976 https://doi.org/10.1021/acschemneuro.9b00179
30 Ban, T., Hamada, D., Hasegawa, K., Naiki, H. and Goto, Y. (2003) Direct observation of amyloid fibril growth monitored by thioflavin T fluorescence. *J. Biol. Chem.* **278**, 16462–16465 https://doi.org/10.1074/jbc.C300049200
31 Andersen, C.B., Yagi, H., Manno, M., Martorana, V., Ban, T., Christiansen, G. et al. (2009) Branching in amyloid fibril growth. *Biophys. J.* **96**, 1529–1536 https://doi.org/10.1016/j.bpj.2008.11.024
32 Wördehoff, M.M., Bannach, O., Shaykhalishahi, H., Kulawik, A., Schiefer, S., Willbold, D. et al. (2015) Single fibril growth kinetics of α-synuclein. *J. Mol. Biol.* **427**, 1428–1435 https://doi.org/10.1016/j.jmb.2015.01.020
33 Young, G., Hundt, N., Cole, D., Fineberg, A., Andrecka, J., Tyler, A. et al. (2018) Quantitative mass imaging of single biological macromolecules. *Science* **360**, 423–427 https://doi.org/10.1126/science.aar5839
34 Meisl, G., Kirkegaard, J.B., Arosio, P., Michaels, T.C.T., Vendruscolo, M., Dobson, C.M. et al. (2016) Molecular mechanisms of protein aggregation from global fitting of kinetic models. *Nat. Protoc.* **11**, 252–272 https://doi.org/10.1038/nprot.2016.010
35 Fränzl, M., Thalheim, T., Adler, J., Huster, D., Posseckardt, J., Mertig, M. et al. (2019) Thermophoretic trap for single amyloid fibril and protein aggregation studies. *Nat. Method* **16**, 611–614 https://doi.org/10.1038/s41592-019-0451-6
36 Cohen, S.I.A., Vendruscolo, M., Dobson, C.M. and Knowles, T.P.J. (2011) Nucleated polymerisation in the presence of pre-formed seed filaments. *Int. J. Mol. Sci.* **12**, 5844–5852 https://doi.org/10.3390/ijms12095844
37 Buell, A.K., Galvagnion, C., Gaspar, R., Sparr, E., Vendruscolo, M., Knowles, T.P.J. et al. (2014) Solution conditions determine the relative importance of nucleation and growth processes in α-synuclein aggregation. *Proc. Natl Acad. Sci. U.S.A.* **111**, 7671–7676 https://doi.org/10.1073/pnas.1315346111
38 Huang, Y.Y., Knowles, T.P.J. and Terentjev, E.M. (2009) Strength of nanotubes, filaments, and nanowires from sonication-induced scission. *Adv. Mater.* **21**, 3945–3948 https://doi.org/10.1002/adma.v21:38/39
39 Collins, S.R., Douglass, A., Vale, R.D. and Weissman, J.S. (2004) Mechanism of prion propagation: amyloid growth occurs by monomer addition. *PLoS Biol.* **2**, e321 https://doi.org/10.1371/journal.pbio.0020321
40 Lorenzen, N., Cohen, S.I.A., Nielsen, S.B., Herling, T.W., Christiansen, G., Dobson, C.M. et al. (2012) Role of elongation and secondary pathways in S6 amyloid fibril growth. *Biophys. J.* **102**, 2167–2175 https://doi.org/10.1016/j.bpj.2012.03.047
41 Xue, W.-F. and Radford, S.E. (2013) An imaging and systems modeling approach to fibril breakage enables prediction of amyloid behavior. *Biophys. J.* **105**, 2811–2819 https://doi.org/10.1016/j.bpj.2013.10.034
42 Honda, R.P. and Kuwata, K. (2017) The native state of prion protein (PrP) directly inhibits formation of PrP-amyloid fibrils in vitro. *Sci. Rep.* **7**, 562 https://doi.org/10.1038/s41598-017-00710-x
43 Kumar, H. and Udgaonkar, J.B. (2018) Mechanistic and structural origins of the asymmetric barrier to prion-like cross-seeding between tau-3R and tau-4R. *J. Mol. Biol.* **430**, 5304–5312 https://doi.org/10.1016/j.jmb.2018.09.010
44 Vavylonis, D., Yang, Q. and O'Shaughnessy, B. (2005) Actin polymerization kinetics, cap structure, and fluctuations. *Proc. Natl Acad. Sci. U.S.A.* **102**, 8543–8548 https://doi.org/10.1073/pnas.0501435102
45 Kuhn, J.R. and Pollard, T.D. (2005) Real-time measurements of actin filament polymerization by total internal reflection fluorescence microscopy. *Biophys. J.* **88**, 1387–1402 https://doi.org/10.1529/biophysj.104.047399
46 Walker, R.A., O'Brien, E.T., Pryer, N.K., Soboeiro, M.F., Voter, W.A., Erickson, H.P. et al. (1988) Dynamic instability of individual microtubules analyzed by video light microscopy: rate constants and transition frequencies. *J. Cell. Biol.* **107**, 1437–1448 https://doi.org/10.1083/jcb.107.4.1437
47 Brännström, K., Öhman, A. and Olofsson, A. (2011) Aβ peptide fibrillar architectures controlled by conformational constraints of the monomer. *PLoS ONE* **6**, e25157 https://doi.org/10.1371/journal.pone.0025157
48 Buell, A.K., Blundell, J.R., Dobson, C.M., Welland, M.E., Terentjev, E.M. and Knowles, T.P.J. (2010) Frequency factors in a landscape model of filamentous protein aggregation. *Phys. Rev. Lett.* **104**, 228101 https://doi.org/10.1103/PhysRevLett.104.228101

49 Buell, A.K., Dhulesia, A., White, D.A., Knowles, T.P.J., Dobson, C.M. and Welland, M.E. (2012) Detailed analysis of the energy barriers for amyloid fibril growth. *Angew. Chem. Int. Ed.* **51**, 5247–5251 https://doi.org/10.1002/anie.201108040

50 Karamanos, T.K., Jackson, M.P., Calabrese, A.N., Goodchild, S.C., Cawood, E.E., Thompson, G.S. et al. (2019) Structural mapping of oligomeric intermediates in an amyloid assembly pathway. *eLife* **8**, e46574 https://doi.org/10.7554/eLife.46574

51 Oncley, J.L., Ellenbogen, E., Gitlin, D. and Gurd, F.R.N. (1952) Protein-protein interactions. *J. Phys. Chem.* **56**, 85–92 https://doi.org/10.1021/j150493a017

52 Yphantis, D.A. and Waugh, D.F. (1957) Dissociation of insulin in pyridine-water and acetic acid-water solutions. *Biochim. Biophys. Acta* **26**, 218–220 https://doi.org/10.1016/0006-3002(57)90082-3

53 Brännström, K., Öhman, A., Nilsson, L., Pihl, M., Sandblad, L. and Olofsson, A. (2014) The N-terminal region of amyloid β controls the aggregation rate and fibril stability at low ph through a gain of function mechanism. *J. Am. Chem. Soc.* **136**, 10956–10964 https://doi.org/10.1021/ja503535m

54 Hellstrand, E., Boland, B., Walsh, D.M. and Linse, S. (2010) Amyloid β-protein aggregation produces highly reproducible kinetic data and occurs by a two-phase process. *ACS Chem. Neurosci.* **1**, 13–18 https://doi.org/10.1021/cn900015v

55 Galvagnion, C., Buell, A.K., Meisl, G., Michaels, T.C.T., Vendruscolo, M., Knowles, T.P.J. et al. (2015) Lipid vesicles trigger α-synuclein aggregation by stimulating primary nucleation. *Nat. Chem. Biol.* **11**, 229–234 https://doi.org/10.1038/nchembio.1750

56 Gaspar, R., Meisl, G., Buell, A.K., Young, L., Kaminski, C.F., Knowles, T.P. et al. (2017) Secondary nucleation of monomers on fibril surface dominates α-synuclein aggregation and provides autocatalytic amyloid amplification. *Quart. Rev. Biophys.* **50**, e6 https://doi.org/10.1017/S0033583516000172

57 Rabe, M., Soragni, A., Reynolds, N.P., Verdes, D., Liverani, E., Riek, R. et al. (2013) On-surface aggregation of α-synuclein at nanomolar concentrations results in two distinct growth mechanisms. *ACS Chem. Neurosci.* **4**, 408–417 https://doi.org/10.1021/cn3001312

58 Asakura, S. (1968) A kinetic study of in vitro polymerization of flagellin. *J. Mol. Biol.* **35**, 237–239 https://doi.org/10.1016/S0022-2836(68)80051-8

59 Milto, K., Botyriute, A. and Smirnovas, V. (2013) Amyloid-like fibril elongation follows michaelis-menten kinetics. *PLoS ONE* **8**, e68684 https://doi.org/10.1371/journal.pone.0068684

60 Esler, W.P., Stimson, E.R., Jennings, J.M., Vinters, H.V., Ghilardi, J.R., Lee, J.P. et al. (2000) Alzheimer's disease amyloid propagation by a template-dependent dock-lock mechanism. *Biochemistry* **39**, 6288–6295 https://doi.org/10.1021/bi992933h

61 Chatani, E., Ohnishi, R., Konuma, T., Sakurai, K., Naiki, H. and Goto, Y. (2010) Pre-steady-state kinetic analysis of the elongation of amyloid fibrils of β2-microglobulin with tryptophan mutagenesis. *J. Mol. Biol.* **400**, 1057–1066 https://doi.org/10.1016/j.jmb.2010.05.071

62 Šarić, A., Buell, A.K., Meisl, G., Michaels, T.C., Dobson, C.M., Linse, S. et al. (2016) Physical determinants of the self-replication of protein fibrils. *Nat. Phys.* **12**, 874–880 https://doi.org/10.1038/nphys3828

63 Cohen, S.I.A., Cukalevski, R., Michaels, T.C.T., Šarić, A., Törnquist, M., Vendruscolo, M. et al. (2018) Distinct thermodynamic signatures of oligomer generation in the aggregation of the amyloid-β peptide. *Nat. Chem.* **10**, 523–531 https://doi.org/10.1038/s41557-018-0023-x

64 Ogi, H., Fukunishi, Y., Yanagida, T., Yagi, H., Goto, Y., Fukushima, M. et al. (2011) Seed-dependent deposition behavior of Aβ peptides studied with wireless quartz-crystal-microbalance biosensor. *Anal. Chem.* **83**, 4982–4988 https://doi.org/10.1021/ac2007703

65 Ogi, H., Fukukshima, M., Hamada, H., Noi, K., Hirao, M., Yagi, H. et al. (2014) Ultrafast propagation of β-amyloid fibrils in oligomeric cloud. *Sci. Rep.* **4**, 6960 https://doi.org/10.1038/srep06960

66 Iadanza, M.G., Jackson, M.P., Radford, S.E. and Ranson, N.A. (2016) Mpul-multi: software for calculation of amyloid fibril mass per unit length from TB-TEM images. *Sci. Rep.* **6**, 21078 https://doi.org/10.1038/srep21078

67 Huxley, H.E. (1963) Electron microscope studies on the structure of natural and synthetic protein filaments from striated muscle. *J. Mol. Biol.* **7**, 281–308 https://doi.org/10.1016/S0022-2836(63)80008-X

68 Pollard, T.D. (1986) Rate constants for the reactions of ATP- and ADP-actin with the ends of actin filaments. *J. Cell. Biol.* **103**, 2747–2754 https://doi.org/10.1083/jcb.103.6.2747

69 DePace, A.H. and Weissman, J.S. (2002) Origins and kinetic consequences of diversity in sup35 yeast prion fibers. *Nat. Struct. Mol. Biol.* **9**, 389–396 https://doi.org/10.1038/nsb786

70 Pinotsi, D., Buell, A.K., Galvagnion, C., Dobson, C.M., Schierle, G.S.K. and Kaminski, C.F. (2013) Direct observation of heterogeneous amyloid fibril growth kinetics via two-color super-resolution microscopy. *Nano Lett.* **14**, 339–345 https://doi.org/10.1021/nl4041093

71 Young, L.J., Kaminski Schierle, G.S. and Kaminski, C.F. (2017) Imaging Aβ(1-42) fibril elongation reveals strongly polarised growth and growth incompetent states. *Phys. Chem. Chem. Phys.* **19**, 27987–27996 https://doi.org/10.1039/C7CP03412A

72 Tuttle, M.D., Comellas, G., Nieuwkoop, A.J., Covell, D.J., Berthold, D.A., Kloepper, K.D. et al. (2016) Solid-state NMR structure of a pathogenic fibril of full-length human α-synuclein. *Nat. Struct. Mol. Biol.* **23**, 409–415 https://doi.org/10.1038/nsmb.3194

73 Levitsky, D.I., Pivovarova, A.V., Mikhailova, V.V. and Nikolaeva, O.P. (2008) Thermal unfolding and aggregation of actin stabilization and destabilization of actin filaments. *FEBS J.* **275**, 4280–4295 https://doi.org/10.1111/j.1742-4658.2008.06569.x

74 Oosawa, F. (1975) *Thermodynamics of the Polymerization of Protein*, Academic Press Inc

75 Gardner, M.K., Charlebois, B.D., Jánosi, I.M., Howard, J., Hunt, A.J. and Odde, D.J. (2011) Rapid microtubule self-assembly kinetics. *Cell* **146**, 582–592 https://doi.org/10.1016/j.cell.2011.06.053

76 Castle, B.T., Odde, D.J. and Woo, D.K. (2019) Rapid and inefficient kinetics of sickle hemoglobin fiber growth. *Sci. Adv.* **5**, eaau1086 https://doi.org/10.1126/sciadv.aau1086

77 Theillet, F.-X., Binolfi, A., Bekei, B., Martorana, A., Rose, H.M., Stuiver, M. et al. (2016) Structural disorder of monomeric α-synuclein persists in mammalian cells. *Nature* **530**, 45–50 https://doi.org/10.1038/nature16531

78 Zurdo, J., Guijarro, J.I., Jimenez, J.L., Saibil, H.R. and Dobson, C.M. (2001) Dependence on solution conditions of aggregation and amyloid formation by an SH3 domain. *J. Mol. Biol.* **311**, 325–340 https://doi.org/10.1006/jmbi.2001.4858

79 Chiti, F. and Dobson, C.M. (2009) Amyloid formation by globular proteins under native conditions. *Nat. Chem. Biol.* **5**, 15–22 https://doi.org/10.1038/nchembio.131

80 Waugh, D.F. (1957) A mechanism for the formation of fibrils from protein molecules. *J. Cell. Comp. Physiol.* **49**, 145–164 https://doi.org/10.1002/(ISSN)1553-0809

81 Buell, A.K., Dhulesia, A., Mossuto, M.F., Cremades, N., Kumita, J.R., Dumoulin, M. et al. (2011) Population of nonnative states of lysozyme variants drives amyloid fibril formation. *J. Am. Chem. Soc.* **133**, 7737–7743 https://doi.org/10.1021/ja109620d

Biochemical Journal (2019) **476** 2677–2703
https://doi.org/10.1042/BCJ20160868

82 Arrhenius, S. (1889) Über die Reaktionsgeschwindigkeit bei der Inversion von Rohrzucker durch Säuren. *Z. Phys. Chem.* **4**, 226–248 https://doi.org/10.1515/zpch-1889-0416

83 Kusumoto, Y., Lomakin, A., Teplow, D.B. and Benedek, G.B. (1998) Temperature dependence of amyloid β-protein fibrillization. *Proc. Natl Acad. Sci. U.S.A.* **95**, 12277–12282 https://doi.org/10.1073/pnas.95.21.12277

84 Vettore, N. and Buell, A. (2019) Thermodynamics of amyloid fibril formation from chemical depolymerization. ChemRxiv (preprint) https://doi.org/10.26434/chemrxiv.9632153.v1

85 Buell, A.K., Dobson, C.M. and Knowles, T.P.J. (2014) The physical chemistry of the amyloid phenomenon: thermodynamics and kinetics of filamentous protein aggregation. *Essays Biochem.* **56**, 11–39 https://doi.org/10.1042/bse0560011

86 White, D.A., Buell, A.K., Knowles, T.P.J., Welland, M.E. and Dobson, C.M. (2010) Protein aggregation in crowded environments. *J. Am. Chem. Soc.* **132**, 5170–5175 https://doi.org/10.1021/ja909997e

87 Linse, S. (2019) Mechanism of amyloid protein aggregation and the role of inhibitors. *Pure Appl. Chem.* **91**, 211–229 https://doi.org/10.1515/pac-2018-1017

88 Waudby, C.A., Knowles, T.P.J., Devlin, G.L., Skepper, J.N., Ecroyd, H., Carver, J.A. et al. (2010) The interaction of αB-crystallin with mature α-synuclein amyloid fibrils inhibits their elongation. *Biophys. J.* **98**, 843–851 https://doi.org/10.1016/j.bpj.2009.10.056

89 Shvadchak, V.V., Afitska, K. and Yushchenko, D.A. (2018) Inhibition of α-synuclein amyloid fibril elongation by blocking fibril ends. *Angew. Chem. Int. Ed.* **57**, 5690–5694 https://doi.org/10.1002/anie.201801071

90 Agerschou, E.D., Flagmeier, P., Saridaki, T., Galvagnion, C., Komnig, D., Heid, L. et al. (2019) An engineered monomer binding-protein for α-synuclein efficiently inhibits the proliferation of amyloid fibrils. *eLife* **8**, e46112 https://doi.org/10.7554/eLife.46112

91 Iljina, M., Hong, L., Horrocks, M.H., Ludtmann, M.H.L., Choi, M.L., Hughes, C.D. et al. (2017) Nanobodies raised against monomeric α-synuclein inhibit fibril formation and destabilize toxic oligomeric species. *BMC Biol.* **15**, 57 https://doi.org/10.1186/s12915-017-0390-6

92 Guilliams, T., El-Turk, F., Buell, A.K., O'Day, E.M., Aprile, F.A., Esbjörner, E.K. et al. (2013) Nanobodies raised against monomeric α-synuclein distinguish between fibrils at different maturation stages. *J. Mol. Biol.* **425**, 2397–2411 https://doi.org/10.1016/j.jmb.2013.01.040

93 Brown, J.W.P., Buell, A.K., Michaels, T.C.T., Meisl, G., Carozza, J., Flagmeier, P. et al. (2016) β-synuclein suppresses both the initiation and amplification steps of α-synuclein aggregation via competitive binding to surfaces. *Sci. Rep.* **6**, 36010 https://doi.org/10.1038/srep36010

94 Lazaridis, T. and Karplus, M. (1997) 'New view' of protein folding reconciled with the old through multiple unfolding simulations. *Science* **278**, 1928–1931 https://doi.org/10.1126/science.278.5345.1928

95 Fersht, A.R. and Sato, S. (2004) Φ-value analysis and the nature of protein-folding transition states. *Proc. Natl Acad. Sci. U.S.A.* **101**, 7976–7981 https://doi.org/10.1073/pnas.0402684101

96 Krebs, M.R.H., Morozova-Roche, L.A., Daniel, K., Robinson, C.V. and Dobson, C.M. (2004) Observation of sequence specificity in the seeding of protein amyloid fibrils. *Protein Sci.* **13**, 1933–1938 https://doi.org/10.1110/(ISSN)1469-896X

97 O'Nuallain, B., Williams, A.D., Westermark, P. and Wetzel, R. (2004) Seeding specificity in amyloid growth induced by heterologous fibrils. *J. Biol. Chem.* **279**, 17490–17499 https://doi.org/10.1074/jbc.M311300200

98 Buell, A.K., Tartaglia, G.G., Birkett, N.R., Waudby, C.A., Vendruscolo, M., Salvatella, X. et al. (2009) Position-dependent electrostatic protection against protein aggregation. *Chembiochem* **10**, 1309–1312 https://doi.org/10.1002/cbic.v10:8

99 Flagmeier, P., Meisl, G., Vendruscolo, M., Knowles, T.P.J., Dobson, C.M., Buell, A.K. et al. (2016) Mutations associated with familial parkinson's disease alter the initiation and amplification steps of α-synuclein aggregation. *Proc. Natl Acad. Sci. U.S.A.* **113**, 10328–10333 https://doi.org/10.1073/pnas.1604645113

100 Bondarev, S., Antonets, K., Kajava, A., Nizhnikov, A. and Zhouravleva, G. (2018) Protein co-aggregation related to amyloids: Methods of investigation, diversity, and classification. *Int. J. Mol. Sci.* **19**, 2292 https://doi.org/10.3390/ijms19082292

101 Chaudhuri, P., Prajapati, K.P., Anand, B.G., Dubey, K. and Kar, K. (2019) Amyloid cross-seeding raises new dimensions to understanding of amyloidogenesis mechanism. *Ageing Res. Rev.*, 100937 https://doi.org/10.1016/j.arr.2019.100937

102 Schierle, G.S.K., van de Linde, S., Erdelyi, M., Esbjörner, E.K., Klein, T., Rees, E. et al. (2011) In situ measurements of the formation and morphology of intracellular β-amyloid fibrils by super-resolution fluorescence imaging. *J. Am. Chem. Soc.* **133**, 12902–12905 https://doi.org/10.1021/ja201651w

103 Pinotsi, D., Michel, C.H., Buell, A.K., Laine, R.F., Mahou, P., Dobson, C.M. et al. (2016) Nanoscopic insights into seeding mechanisms and toxicity of α-synuclein species in neurons. *Proc. Natl Acad. Sci. U.S.A.* **113**, 3815–3819 https://doi.org/10.1073/pnas.1516546113

104 Rogers, S.S., Krebs, M.R.H., Bromley, E.H.C., van der Linden, E. and Donald, A.M. (2006) Optical microscopy of growing insulin amyloid spherulites on surfaces in vitro. *Biophys. J.* **90**, 1043–1054 https://doi.org/10.1529/biophysj.105.072660

105 van der Wateren, I.M., Knowles, T., Buell, A., Dobson, C.M. and Galvagnion, C. (2018) C-terminal truncation of α-synuclein promotes amyloid fibril amplification at physiological pH. *Chem. Sci.* **9**, 5506–5516 https://doi.org/10.1039/C8SC01109E

106 Meisl, G., Yang, X., Hellstrand, E., Frohm, B., Kirkegaard, J.B., Cohen, S.I.A. et al. (2014) Differences in nucleation behavior underlie the contrasting aggregation kinetics of the Aβ40 and Aβ42 peptides. *Proc. Natl Acad. Sci. U.S.A.* **111**, 9384–9389 https://doi.org/10.1073/pnas.1401564111

107 Drenckhahn, D. and Pollard, T.D. (1986) Elongation of actin filaments is a diffusion-limited reaction at the barbed end and is accelerated by inert macromolecules. *J. Biol. Chem.* **261**, 12754–12758

108 Aprelev, A., Liu, Z. and Ferrone, F.A. (2011) The growth of sickle hemoglobin polymers. *Biophys. J.* **101**, 885–891 https://doi.org/10.1016/j.bpj.2011.05.064

109 von Smoluchowski, M. (1917) Versuch einer mathematischen Theorie der Koagulationskinetik kolloider Lösungen. *Z. Phys. Chem.* **92**, 129 https://doi.org/10.1515/zpch-1918-9209

110 Ferkinghoff-Borg, J., Fonslet, J., Andersen, C.B., Krishna, S., Pigolotti, S., Yagi, H. et al. (2010) Stop-and-go kinetics in amyloid fibrillation. *Phys. Rev. E* **82**, 010901 https://doi.org/10.1103/PhysRevE.82.010901

111 Cohen, S.I.A., Linse, S., Luheshi, L.M., Hellstrand, E., White, D.A., Rajah, L. et al. (2013) Proliferation of amyloid-β42 aggregates occurs through a secondary nucleation mechanism. *Proc. Natl Acad. Sci. U.S.A.* **110**, 9758–9763 https://doi.org/10.1073/pnas.1218402110

112 Goldsbury, C., Frey, P., Olivieri, V., Aebi, U. and Müller, S.A. (2005) Multiple assembly pathways underlie amyloid-β fibril polymorphisms. *J. Mol. Biol.* **352**, 282–298 https://doi.org/10.1016/j.jmb.2005.07.029

113 Qiang, W., Kelley, K. and Tycko, R. (2013) Polymorph-specific kinetics and thermodynamics of β-amyloid fibril growth. *J. Am. Chem. Soc.* **135**, 6860–6871 https://doi.org/10.1021/ja311963f

114 Ban, T., Hoshino, M., Takahashi, S., Hamada, D., Hasegawa, K., Naiki, H. et al. (2004) Direct observation of Aβ amyloid fibril growth and inhibition. *J. Mol. Biol.* **344**, 757–767 https://doi.org/10.1016/j.jmb.2004.09.078
115 Patil, S.M., Mehta, A., Jha, S. and Alexandrescu, A.T. (2011) Heterogeneous amylin fibril growth mechanisms imaged by total internal reflection fluorescence microscopy. *Biochemistry* **50**, 2808–2819 https://doi.org/10.1021/bi101908m
116 Ban, T. and Goto, Y. (2006) Direct observation of amyloid growth monitored by total internal reflection fluorescence microscopy. *Methods Enzymol.* **413**, 91–102 https://doi.org/10.1016/S0076-6879(06)13005-0
117 Bhattacharyya, A.M., Thakur, A.K. and Wetzel, R. (2005) Polyglutamine aggregation nucleation: thermodynamics of a highly unfavorable protein folding reaction. *Proc. Natl Acad. Sci. U.S.A.* **102**, 15400–15405 https://doi.org/10.1073/pnas.0501651102
118 Kar, K., Jayaraman, M., Sahoo, B., Kodali, R. and Wetzel, R. (2011) Critical nucleus size for disease-related polyglutamine aggregation is repeat-length dependent. *Nat. Struct. Mol. Biol.* **18**, 328–336 https://doi.org/10.1038/nsmb.1992
119 Kar, K., Hoop, C.L., Drombosky, K.W., Baker, M.A., Kodali, R., Arduini, I. et al. (2013) β-hairpin-mediated nucleation of polyglutamine amyloid formation. *J. Mol. Biol.* **425**, 1183–1197 https://doi.org/10.1016/j.jmb.2013.01.016
120 Wang, Y.-Q., Buell, A.K., Wang, X.-Y., Welland, M.E., Dobson, C.M., Knowles, T.P.J. et al. (2011) Relationship between prion propensity and the rates of individual molecular steps of fibril assembly. *J. Biol. Chem.* **286**, 12101–12107 https://doi.org/10.1074/jbc.M110.208934
121 Andreasen, M., Meisl, G., Taylor, J.D., Michaels, T.C.T., Levin, A., Otzen, D.E. et al. (2019) Physical determinants of amyloid assembly in biofilm formation. *Mbio* **10**, e02279-18 https://doi.org/10.1128/mBio.02279-18
122 Sleutel, M., Van den Broeck, I., Van Gerven, N., Feuillie, C., Jonckheere, W., Valotteau, C. et al. (2017) Nucleation and growth of a bacterial functional amyloid at single-fiber resolution. *Nat. Chem. Biol.* **13**, 902–908 https://doi.org/10.1038/nchembio.2413
123 Cooper, J.A., Walker, S.B. and Pollard, T.D. (1983) Pyrene actin: documentation of the validity of a sensitive assay for actin polymerization. *J. Muscle Res. Cell Motility* **4**, 253–262 https://doi.org/10.1007/BF00712034
124 Lal, A.A., Brenner, S. and Korn, E.D. (1984) Preparation and polymerization of skeletal muscle ADP-actin. *J. Biol. Chem.* **259**, 13061–13065
125 Carrotta, R., Manno, M., Bulone, D., Martorana, V. and Biagio, P.L.S. (2005) Protofibril formation of amyloid β-protein at low pH via a non-cooperative elongation mechanism. *J. Biol. Chem.* **280**, 30001–30008 https://doi.org/10.1074/jbc.M500052200
126 Sabate, R., Castillo, V., Espargaro, A., Saupe, S.J. and Ventura, S. (2009) Energy barriers for HET-s prion forming domain amyloid formation. *FEBS J.* **276**, 5053–5064 https://doi.org/10.1111/j.1742-4658.2009.07202.x
127 Skerget, K., Vilfan, A., Pompe-Novak, M., Turk, V., Waltho, J.P., Turk, D. et al. (2009) The mechanism of amyloid-fibril formation by stefin B: temperature and protein concentration dependence of the rates. *Proteins* **74**, 425–436 https://doi.org/10.1002/prot.v74:2
128 Kim, Y.-S., Randolph, T.W., Stevens, F.J. and Carpenter, J.F. (2002) Kinetics and energetics of assembly, nucleation, and growth of aggregates and fibrils for an amyloidogenic protein. Insights into transition states from pressure, temperature, and co-solute studies. *J. Biol. Chem.* **277**, 27240–27246 https://doi.org/10.1074/jbc.M202492200
129 Kasai, M. (1969) Thermodynamical aspect of G-F transformations of actin. *Biochim. Biophys. Acta* **180**, 399–409 https://doi.org/10.1016/0005-2728(69)90124-8
130 Zimmerle, C.T. and Frieden, C. (1986) Effect of temperature on the mechanism of actin polymerization. *Biochemistry* **25**, 6432–6438 https://doi.org/10.1021/bi00369a014
131 Johnson, K.A. (1980) Thermodynamics of microtubule assembly. *Biophys. J.* **32**, 443–445 https://doi.org/10.1016/S0006-3495(80)84975-7
132 Choudhury, G.G., Bhattacharyya, B. and Biswas, B.B. (1987) Kinetic and thermodynamic analysis of taxol-induced polymerization of purified tubulin. *Biochem. Cell. Biol.* **65**, 558–564 https://doi.org/10.1139/o87-072
133 Eyring, H. (1935) The activated complex in chemical reactions. *J. Chem. Phys.* **3**, 107–115 https://doi.org/10.1063/1.1749604
134 Kramers, H.A. (1940) Brownian motion in a field of force and the diffusion model of chemical reactions. *Physica* **7**, 284–304 https://doi.org/10.1016/S0031-8914(40)90098-2